Iron(II) and Cobalt(II) 2-(Benzimidazolyl)-6-(1-(arylimino)ethyl)pyridyl Complexes as Catalysts for Ethylene Oligomerization and Polymerization

Wen-Hua Sun,* Peng Hao, Shu Zhang, Qisong Shi, Weiwei Zuo, and Xiubo Tang

Key Laboratory of Engineering Plastics and Beijing National Laboratory for Molecular Sciences, Institute of Chemistry, Chinese Academy of Sciences, Beijing 100080, People's Republic of China

Xiaoming Lu

Department of Chemistry, Capital Normal University, Beijing 100037, People's Republic of China

Received January 28, 2007

A series of iron(II) (**7a**−**11a**) and cobalt(II) (**7b**−**11b**) 2-(1-methyl-2-benzimidazolyl)-6-(1-(arylimino)-ethyl)pyridyl complexes were synthesized, as well as bidentate iron(II) and cobalt(II) complexes ligated by 2-(2-benzimidazolyl)-6-methylpyridine, 2-(carboethoxyl)-6-(2-benzimidazolyl)pyridine, and 2-(1-methyl-2-benzimidazolyl)-6-acetylpyridine. All organic compounds were fully characterized by NMR and IR spectroscopy and elemental analysis, while the metal complexes were carefully examined by IR spectroscopy and elemental analysis. Their molecular structures were determined by single-crystal X-ray diffraction analysis. The bidentate metal complexes display a distorted-tetrahedral coordination geometry; however, **2a** is an exception, with a distorted-trigonal-bipyramidal geometry due to coordination of one DMF molecule. The X-ray crystallographic studies on all of the tridentate metal complexes revealed the coordination geometry as a distorted trigonal bipyramid. Upon activation with MAO or MMAO, the iron(II) 2-(2-benzimidazolyl)-6-(1-(arylimino)ethyl)pyridyl complexes showed high activities with good α-olefin selectivity, while the cobalt(II) analogues displayed moderate to good catalytic activities. However, other bidentate metal complexes showed considerable moderate catalytic activity. The oligomers and polyethylene waxes obtained were α-olefins, and the distribution of oligomers resembled Schulz−Flory rules with some exceptions. Various reaction parameters were investigated, and the results revealed that both the steric and electronic effects of ligands affect the catalytic activities of their metal complexes as well as the distribution of products.

1. Introduction

The US market for polyolefins and α-olefins is in the tens of billions of dollars, both indicating their importance and stimulating interest in academic and industrial research in this field. Polyolefins, with an annual market of over 110 million tons, are half the volume of all synthesized plastics.[1] Linear α-olefins, on the other hand, with more than 5 million tons annual production, are important substances used in the preparation of detergents, lubricants, plasticizers, oil field chemicals, and monomers for copolymerization. One challenge is to design catalysts with higher catalytic activity and performance for advanced polyolefins. With ethylene as the feedstock, ethylene activation has provided fast-growing polyethylenes made up of 60% polyolefins and is the major source of linear α-olefins (a range of C_4/C_6 up to C_{20+}). The industrial processes of ethylene polymerization have developed with catalysts of titanium,[2] chromium,[2b,3] and recently zirconium,[4] while the processes of ethylene oligomerization (including on purpose and full range) have been achieved with the Ziegler (Alfen) process,[5] chromium-based complexes[6] and the Shell Higher Olefin Process (SHOP).[7] Breakthroughs in organometallic chemistry and its catalytic applications have completely transformed our view of designing new complexes as Robot catalysts for ethylene oligomerization and polymerizations. The rapid progress in the use of metal complexes have been termed a "metal complex revolution" for ethylene activation. First, metallocenes (zirconocene and half-metallocene) were used as single-site catalysts in the 1980s,[4c,d,8] followed by late-transition-metal catalysts[9] in the mid-1990s; at present, various catalysts of complexes of early[10] and late transition metals dominate the scene. However, the strong defect of "deactivation" caused by the oxophilicity of early-transition-

* To whom correspondence should be addressed. Tel: +86 10 62557955. Fax: +86 10 62618239. E-mail: whsun@iccas.ac.cn.

(1) Galli, P.; Vecellio, G. *J. Polym. Sci. A: Polym. Chem.* **2004**, *42*, 396.

(2) (a) Fink, G.; Mülhaupt, R.; Brintzinger, H. H. In *Ziegler Catalysts*; Springer-Verlag: Berlin, Heidelberg, Germany, 1999. (b) Pullukat, T. J.; Hoff, R. E. *Catal. Rev. Sci. Eng.* **1999**, *41*, 389.

(3) (a) Weckhuysen, B. M.; Schoonheydt, R. A. *Catal. Today* **1999**, *51*, 215. (b) Fang, Y.; Liu, B.; Terano, M. *Kinet. Catal.* **2006**, *47*, 295.

(4) (a) Brintzinger, H. H.; Fischer, D.; Mulhaupt, R.; Rieger, B.; Waymouth, R. M. *Angew. Chem., Int. Ed. Engl.* **1995**, *34*, 1143. (b) Coates, G. W. *Chem. Rev.* **2000**, *100*, 1223. (c) Alt, H. G.; Köppl, A. *Chem. Rev.* **2000**, *100*, 1205. (d) Kaminsky, W. *J. Polym. Sci., Part A: Polym. Chem.* **2004**, *42*, 3911.

(5) (a) Zieger, K.; Martin, H. U.S. Patent 2,943,125, 1954. (b) Al-Jarallah, A. M.; Anabtawi, J. A.; Siddiqui, M. A. B.; Aitani, A. M. *Catal. Today* **1992**, *14*, 1.

(6) (a) Reagen, W. K. *Am. Chem. Soc. Symp., Div. Petroleum Chem.* **1989**, *34*, 583, 3. (b) Reagen, W. K.; Conroy, B. K. (Phillips Petroleum) U.S. Patent 5,288,823, 1994. (c) Bollmann, A.; Blann, K.; Dixon, J. T.; Hess, F. M.; Killian, E.; Maumela, H.; McGuinness, D. S.; Morgan, D. H.; Neveling, A.; Otto, S.; Overett, M.; Slawin, A. M. Z.; Wasserscheid, P.; Kuhlmann, S. *J. Am. Chem. Soc.* **2004**, *126*, 14712. (d) Overett, M. J.; Blann, K.; Bollmann, A.; Dixon, J. T.; Hess, F.; Killian, E.; Maumela, H.; Morgan, D. H.; Neveling, A.; Otto, S. *Chem. Commun.* **2005**, 622.

10.1021/om0700819 CCC: $37.00
Publication on Web 04/04/2007

metal complexes during storage paved the way for stable late-transition-metal complexes as catalysts for ethylene reactivity with the expectation of high activity.

The strategy of late-transition-metal catalysts in olefin activation started with the "nickel effect" in the 1950s, and optimization of the reaction conditions resulted in the development of the SHOP process. In contrast to the case for the development of early-transition-metal catalysts, the late-transition-metal catalysts have been less investigated because of major β-hydrogen elimination occurring in competition with ethylene insertion and chain propagation of the polymer. The resurrection of late-transition-metal catalysts was initially induced by the development of bidentate nickel and palladium diimino halides by the Brookhart group,[11] and tridentate iron and cobalt 2,6-bis(imino)pyridyl halides by both the Brookhart group[12] and the Gibson group.[13] Late-transition-metal complexes as catalysts for ethylene oligomerization and polymerization have currently drawn much attention in the design of new catalysts and optimization of the standard catalyst models.[14] The progress in the use of late-transition-metal catalysts has been well documented with reviews[9,15] and extensively investigated, with insights into their active intermediates and catalytic mechanism.[16] In addition to ethylene polymerization, there is the longstanding consideration and promising application of late-transition-metal catalysts to ethylene oligomerization for linear α-olefins;[14a] in addition, iron catalysts have shown the advantages of high activities and exceptional selectivity of α-olefins to produce new olefin waxes.[14a,17] The valuable catalysts are potentially useful as new drop-in catalysts in the current commercial processes operated by BP, Chevron Phillips, and Shell.[18] Apart from iron(II) catalysts ligated by bis(imino)-pyridines, a few new models of iron catalysts were reported to have limited activity,[19] but iron complexes based on 1,10-phenanthroline[20] provided an alternative iron model with very high activity.[21] During our extensive research on metal complexes with iminopyridines,[22] 2-imino-1,10-phenanthrolines,[23] and 2,6-bis(2-benzimidazole)pyridines,[24] a new challenge has been to develop a catalyst model of complexes bearing novel ligands as the hybrids of bis(1-(arylimino)ethyl)pyridines and bis(2-benzimidazolyl)pyridines, 2-(benzimidazolyl)-6-(1-(arylimino)ethyl)pyridines. The proposed metal complexes ligated by

(7) (a) Keim, W.; Kowaldt, F. H.; Goddard, R.; Krüger, C. *Angew. Chem.* **1978**, *90*, 493; *Angew. Chem., Int. Ed. Engl.* **1978**, *17*, 466. (b) Keim, W.; Behr, A.; Limbacker, B.; Krüger, C. *Angew. Chem., Int. Ed. Engl.* **1983**, *22*, 503. (c) Keim, W.; Behr, A.; Kraus, G. *J. Organomet. Chem.* **1983**, *251*, 377. (d) Grenouillet, P.; Neibecker, D.; Tkatchenko, I. *J. Organomet. Chem.* **1983**, *243*, 213. (e) Peuckert, M.; Keim, W. *Organometallics* **1983**, *2*, 594. (f) Peuckert, M.; Keim, W. *J. Mol. Catal.* **1984**, *22*, 289. (g) Keim, W. *New J. Chem.* **1987**, *11*, 531. (h) Klabunde, U.; Itten, S. D. *J. Mol. Catal.* **1987**, *41*, 123. (i) Ostoja Starzewski, K. A.; Witte, J. *Angew. Chem.* **1987**, *99*, 76; *Angew. Chem., Int. Ed. Engl.* **1987**, *26*, 63. (j) Keim, W. *Angew. Chem.* **1990**, *102*, 251; *Angew. Chem., Int. Ed. Engl.* **1990**, *29*, 235. (k) Hirose, K.; Keim, W. *J. Mol. Catal.* **1992**, *73*, 271. (l) Keim, W. *Macromol. Chem. Macromol. Symp.* **1993**, *66*, 225. (m) Matt, D.; Huhn, M.; Fischer, J.; De Cian, A.; Kläui, W.; Tkatchenlo, I.; Bonnet, M. C. *J. Chem. Soc., Dalton Trans.* **1993**, 1173. (n) Keim, W.; Schulz, R. P. *J. Mol. Catal.* **1994**, *92*, 21. (o) Braunstein, P.; Chauvin, Y.; Mecier, S.; Saussine, L.; De Cian, A.; Fischer, J. *J. Chem. Soc., Chem. Commun.* **1994**, 2203.

(8) Sinn, H.; Kaminsky, W.; Vollmer, H.-J.; Woldt, R. *Angew. Chem., Int. Ed. Engl.* **1980**, *19*, 390.

(9) (a) Britovsek, G. J. P.; Gibson, V. C.; Wass, D. F. *Angew. Chem., Int. Ed.* **1999**, *38*, 428. (b) Ittel, S. D.; Johnson, L. K.; Brookhart, M. *Chem. Rev.* **2000**, *100*, 1169. (c) Gibson, V. C.; Spitzmesser, S. K. *Chem. Rev.* **2003**, *103*, 283. (d) Sun, W.-H.; Zhang, D.; Zhang, S.; Jie, S.; Hou, J. *Kinet. Catal.* **2006**, *47*, 278. (e) Jie, S.; Zhang, S.; Sun, W.-H. *Shiyou Huagong* **2006**, *35*, 297.

(10) (a) Mitani, M.; Mohri, J.; Yoshida, Y.; Saito, J.; Ishii, S.; Tsuru, K.; Matsui, S.; Furuyama, R.; Nakano, T.; Tanaka, H.; Kojoh, S.; Matsugi, T.; Kashiwa, N.; Fujita, T. *J. Am. Chem. Soc.* **2002**, *124*, 3327. (b) Volkis, V.; Nelkenbaum, E.; Lisovskii, A.; Hasson, G.; Semiat, R.; Kapon, M.; Botoshansky, M.; Eishen, Y.; Eisen, M. S. *J. Am. Chem. Soc.* **2003**, *125*, 2179. (c) Yoshida, Y.; Mohri, J.; Ishii, S.; Mitani, M.; Saito, J.; Matsui, S.; Makio, H.; Nakano, T.; Tanaka, H.; Onda, M.; Yamamoto, Y.; Mizuno, A.; Fujita, T. *J. Am. Chem. Soc.* **2004**, *126*, 12023.

(11) (a) Johnson, L. K.; Killian, C. M.; Brookhart, M. *J. Am. Chem. Soc.* **1995**, *117*, 6414. (b) Svejda, S. A.; Brookhart, M. *Organometallics* **1999**, *18*, 65. (c) Killian, C. M.; Johnson, L. K.; Brookhart, M. *Organometallics* **1997**, *16*, 2005.

(12) Small, B. L.; Brookhart, M.; Bennett, A. M. A. *J. Am. Chem. Soc.* **1998**, *120*, 4049.

(13) Britovsek, G. J. P.; Gibson, V. C.; Kimberley, B. S.; Maddox, P. J.; McTavish, S. J.; Solan, G. A.; White, A. J. P.; Williams, D. J. *Chem. Commun.* **1998**, 849.

(14) (a) Ionkin, A. S.; Marshall, W. J.; Adelman, D. J.; Fones, B. B.; Fish, B. M.; Schiffhauer, M. F. *Organometallics* **2006**, *25*, 2978. (b) Schrekker, H. S.; Kotov, V.; Preishuber-Pflugl, P.; White, P.; Brookhart, M. *Macromolecules* **2006**, *39*, 6341. (c) Taquet, J. P.; Siri, O.; Braunstein, P.; Welter, R. *Inorg. Chem.* **2006**, *45*, 4668.

(15) (a) Speiser, F.; Braunstein, P.; Saussine, L. *Acc. Chem. Res.* **2005**, *38*, 784. (b) Mecking, S. *Angew. Chem., Int. Ed.* **2001**, *40*, 534. (c) Stapleton, R. L.; Chai, J.; Taylor, N. J.; Collins, S. *Organometallics* **2006**, *25*, 2514. (d) Sui-Seng, C.; Castonguay, A.; Chen, Y.; Gareau, D.; Groux, L. F.; Zargarian, D. *Top. Catal.* **2006**, *37*, 81.

(16) (a) Heinicke, J.; Köhler, M.; Peulecke, N.; Kindermann, M. K.; Keim, W.; Köckerling, M. *Organometallics* **2005**, *24*, 344. (b) Chen, Y. F.; Wu, G.; Bazan, G. C. *Angew. Chem., Int. Ed.* **2005**, *44*, 1108. (c) Britovsek, G. J. P.; England, J.; Spitzmesser, S. K.; White, A. J. P.; Williams, D. J. *Dalton Trans.* **2005**, 945. (d) Wang, Q.; Li, L. D.; Fan, Z. Q. *J. Polym. Sci. A: Polym. Chem.* **2005**, *43*, 1599. (e) Blackmore, I. J.; Gibson, V. C.; Hitchcock, P. B.; Rees, C. W.; Williams, D. J.; White, A. J. P. *J. Am. Chem. Soc.* **2005**, *127*, 6012. (f) Humphries, M. J.; Tellmann, K. P.; Gibson, V. C.; White, A. J. P.; Williams, D. J. *Organometallics* **2005**, *24*, 2039. (g) Bouwkamp, M. W.; Lobkovsky, E.; Chirik, P. J. *J. Am. Chem. Soc.* **2005**, *127*, 9660. (h) Kleigrewe, N.; Steffen, W.; Blömker, T.; Kehr, G.; Fröhlich, R.; Wibbeling, B.; Erker, G.; Wasilke, J.-C.; Wu, G.; Bazan, G. C. *J. Am. Chem. Soc.* **2005**, *127*, 13955. (i) Scott, J.; Gambarotta, S.; Korobkov, I.; Knijnenburg, Q.; de Bruin, B.; Budzelaar, P. H. M. *J. Am. Chem. Soc.* **2005**, *127*, 17204. (j) Wang, S. B.; Liu, D. B.; Huang, R. B.; Zhang, Y. D.; Mao, B. Q. *J. Mol. Catal. A* **2006**, *245*, 122. (k) Zhang, L.; Brookhart, M.; White, P. S. *Organometallics* **2006**, *25*, 1868. (l) Rose, J. M.; Cherian, A. E.; Coates, G. W. *J. Am. Chem. Soc.* **2006**, *128*, 4186.

(17) (a) Kerbow, D. L.; Schiffino, R. S.; Culver, D. A.(E. I. du Pont de Nemours) U.S. Patent 7,053,259, May 30, 2006 (priority date Sept 8, 2003). (b) Heilman, W. J.; Chiu, I-C.; Chien, J. C. W. (Penzoil-Quaker State Company) U.S. Patent 6,730,818, May 4, 2004 (priority date May 22, 2002). (c) Ravindranathan, M.; Pillai, S. M.; Tembe, G. L. (Pillsbury Winthrop Shaw Pittman LLP) U.S. Patent 6,930,218, Aug 16, 2005 (priority date Aug 23, 2001). (d) Small, B. L.; Carney, M. J.; Holman, D. M.; O'Rourke, C. E.; Halfen, J. A. *Macromolecules* **2004**, *37*, 4375.

(18) (a) Vogt, D. In *Applied Homogeneous Catalysis with Organometallic Compounds*; Cornils, B., Herrmann, W. A., Eds.; VCH: Weinheim, Germany, 2002; Vol. 1, p 240. (b) Parshall, G. W.; Ittel, S. D. In *Homogeneous Catalysis: The Applications and Chemistry of Catalysis by Soluble Transition Metal Complexes*; Wiley: New York, 1992; p 68.

(19) (a) Qian, M.; Wang, M.; He, R. *J. Mol. Catal. A* **2000**, *160*, 243. (b) LePichon, L.; Stephan, D. W.; Gao, X.; Wang, Q. *Organometallics* **2002**, *21*, 1362. (c) Bianchini, C.; Mantovani, G.; Meli, A.; Migliacci, F.; Laschi, F. *Organometallics* **2003**, *22*, 2545. (d) Zhou, M.-S.; Huang, S.-P.; Weng, L.-H.; Sun, W.-H.; Liu, D.-S. *J. Organomet. Chem.* **2003**, *665*, 237. (e) Britovsek, G. J. P.; Gibson, V. C.; Hoarau, O. D.; Spitzmesser, S. K.; White, A. J. P.; Williams, D. J. *Inorg. Chem.* **2003**, *42*, 3454. (f) Cowdell, R.; Davies, C. J.; Hilton, S. J.; Maréchal, J.-D.; Solan, G. A.; Thomas, O.; Fawcett, J. *Dalton Trans.* **2004**, 3231. (g) Sun, W.-H.; Tang, X.; Gao, T.; Wu, B.; Zhang, W.; Ma, H. *Organometallics* **2004**, *23*, 5037.

(20) (a) Wang, L.; Sun, W.-H.; Han, L.; Yang, H.; Hu, Y.; Jin, X. *J. Organomet. Chem.* **2002**, *658*, 62. (b) Britovsek, G. J. P.; Baugh, S. P. D.; Hoarau, O.; Gibson, V. C.; Wass, D. F.; White, A. J. P.; Williams, D. J. *Inorg. Chim. Acta* **2003**, *345*, 279.

(21) Sun, W.-H.; Jie, S.; Zhang, S.; Zhang, W.; Song, Y.; Ma, H.; Chen, J.; Wedeking, K.; Fröhlich, R. *Organometallics* **2006**, *25*, 666.

(22) (a) Tang, X.; Sun, W.-H.; Gao, T.; Hou, J.; Chen, J.; Chen, W. *J. Organomet. Chem.* **2005**, *690*, 1570. (b) Jie, S.; Zhang, D.; Zhang, T.; Sun, W.-H.; Chen, J.; Ren, Q.; Liu, D.; Zheng, G.; Chen, W. *J. Organomet. Chem.* **2005**, *690*, 1739. (c) Hou, J.; Sun, W.-H.; Zhang, S.; Ma, H.; Deng, Y.; Lu, X. *Organometallics* **2006**, *25*, 236. (d) Zhang, W.; Sun, W.-H.; Wu, B.; Zhang, S.; Ma, H; Li, Y.; Chen, J.; Hao, P. *J. Organomet. Chem.* **2006**, *691*, 4759.

(23) (a) Sun, W.-H.; Zhang, S.; Jie, S.; Zhang, W.; Li, Y.; Ma, H.; Chen, J.; Wedeking, K.; Fröhlich, R. *J. Organomet. Chem.* **2006**, *691*, 4196. (b) Jie, S.; Zhang, S.; Wedeking, K.; Zhang, W.; Ma, H.; Lu, X.; Deng, Y.; Sun, W.-H. *C. R. Chim.* **2006**, *9*, 1500.

(24) Zhang, W.; Sun, W.-H.; Zhang, S.; Hou, J.; Wedeking, K.; Schultz, S.; Fröhlich, R.; Song, H. *Organometallics* **2006**, *25*, 1961.

2-(benzimidazolyl)-6-(1-(arylimino)ethyl)pyridines would potentially have the advantage of high activities and flexibilities in producing α-olefins or α-olefin waxes through adapting their structural features. To verify this hypothesis, a convenient synthetic methodology was developed to prepare the ligand model of 2-(2-benzimidazolyl)-6-acetylpyridine in good yield on the laboratory scale of tens of grams through intermediate compounds of 2-(2-benzimidazolyl)-6-methylpyridine and 2-(carboethoxyl)-6-(2-benzimidazolyl)pyridine. The 2-(benzimidazolyl)-6-(1-(arylimino)ethyl)pyridines were routinely prepared by the condensation reactions of 2-(2-benzimidazolyl)-6-acetylpyridine with corresponding substituted anilines; thereafter, their iron and cobalt complexes were synthesized and characterized. As expected, upon activation with organoaluminum, the catalytic systems of 2-(benzimidazolyl)-6-(1-(arylimino)ethyl)-pyridyl complexes demonstrated very high activities in ethylene oligomerization and polymerization to produce α-olefins and waxes. In addition, metal complexes ligated by 2-(2-benzimidazolyl)-6-methylpyridine, 2-(carboethoxyl)-6-(2-benzimidazolyl)-pyridine, and 2-(1-methyl-2-benzimidazolyl)-6-acetylpyridine were also synthesized and characterized, and their catalytic performance in ethylene activation was examined. Herein the synthesis and characterization of 2-(1-methyl-2-benzimidazolyl)-6-(1-(arylimino)ethyl) pyridines and their synthetic intermediates as well as of their iron and cobalt complexes are reported, along with a detailed investigation of the catalytic behavior of metal complexes to ethylene activation under various reaction conditions.

2. Results and Discussion

2.1. Preparation of 2-(1-Methyl-2-benzimidazole)-6-acetylpyridine and Its Synthetic Intermediates. The design of functional organic compounds as suitable ligands is an interesting prerequisite for new complexes in coordination chemistry and homogeneous catalysis. In order to obtain 2-(2-benzimidazole)-6-acetylpyridine, with two functional groups, it is necessary to employ multistep synthetic procedures. The literature synthetic methods for constructing 2-benzimidazolylpyridine include the condensation reaction of *o*-phenylenediamine and pyridine-2-carboxylic acid in the presence of phosphoric acid (PPA)[25] or the oxidation reaction by sulfur of *o*-phenylenediamine and 2,6-lutidine.[26] Accordingly, the solid reaction of *o*-phenylenediamine and 2,6-lutidine in the presence of sulfur oxidant was employed to prepare 2-(2-benzimidazolyl)-6-methylpyridine (**1**) in an acceptable yield.[26] Though several oxide reagents were tried, it was necessary to use SeO_2 in the oxidation of 2-(2-benzimidazolyl)-6-methylpyridine (**1**) into 6-(2-benzimidazolyl)pyridine-2-carboxylic acid (**3**).[27] In the presence of a catalytic amount of H_2SO_4, its esterification with ethanol was carried out to form 2-(carboethoxy)-6-(2-benzimidazolyl)pyridine (**4**).[19g,28] Perhaps due to the reaction of benzimidazole with a strong base, the transformation of its carboxylate into an acetyl group to form 6-(2-benzimidazolyl)-2-acetylpyridine could not be achieved by direct reflux with ethyl acetate in the presence of C_2H_5ONa and the following workup. Therefore, the N-methylation of the 2-benzimidazolyl compound to 2-(carboethoxy)-6-(1-methyl-2-benzimidazolyl)pyridine (**5**) was carried out with the reaction of methyl iodide in acetonitrile and K_2CO_3 at room temperature.[29] Then, the routine transformation of a carboxylate group into an acetyl group,[19g] through a Claisen reaction with ethyl acetate under basic conditions and then proceeding in acidic solution, gave 2-(1-methyl-2-benzimidazolyl)-6-acetylpyridine (**6**) in an appropriate yield. Similarly, 2-(1-methyl-2-benzimidazolyl)-6-methylpyridine (**2**) was also synthesized in good yield through the N-methylation reaction. All synthesized compounds were well characterized and confirmed by elemental analysis and ^1H and ^{13}C NMR and IR spectrometry. The synthetic procedures from 2,6-lutidine to 6-(1-methyl-2-benzimidazolyl)-2-acetylpyridine are summarized in Scheme 1.

Scheme 1. Synthesis of 2-(1-Methyl-2-benzimidazolyl)-6-acetylpyridine and Its Intermediates

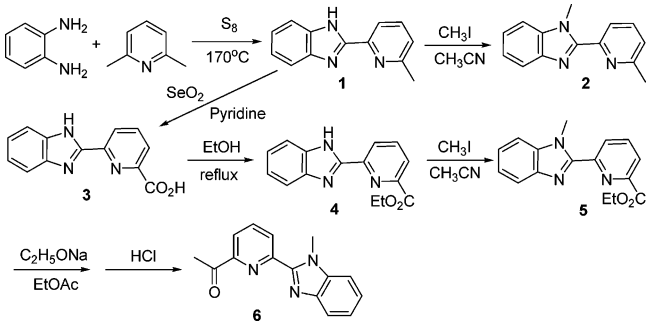

Scheme 2. Reaction of MCl_2 with 2-(Benzimidazolyl)pyridine Derivatives

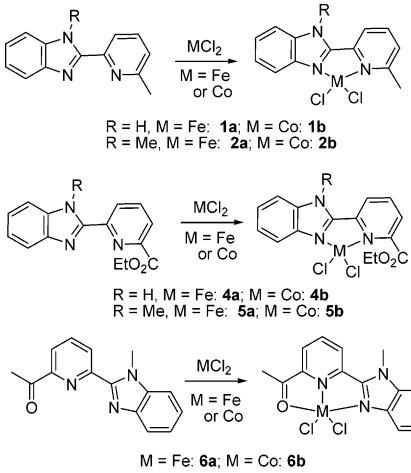

2.2. Synthesis and Characterization of Iron and Cobalt Complexes Bearing Various 6-Substituted 2-Benzimidazolylpyridines. The synthesized 6-substituted 2-benzimidazolylpyridine derivatives 2-(1-R′-2-benzimidazolyl)-6-R″-pyridine (R′ = H, R″ = Me, **1**; R′ = Me, R″ = Me, **2**; R′ = H, R″ = carboethoxyl, **4**; R′ = Me, R″ = carboethoxyl, **5**; R′ = Me, R″ = acetyl, **6**) could be good bidentate or tridentate ligands for coordination with transition metals. Guided by our previous works on bidentate iron and cobalt catalysts for ethylene activation,[22,30] the complexes were synthesized in proper yields by equimolar reactions of the synthesized 2-benzimidazolylpyridine derivatives with $FeCl_2 \cdot 4H_2O$ or $CoCl_2$ in ethanol (Scheme 2).

These complexes were characterized by elemental analysis and IR spectrometry. In comparison with the IR spectrometry

(25) Barni, E.; Savarino, P. *J. Heterocycl. Chem.* **1977**, *14*, 937.
(26) Tsukamoto, G.; Yoshino, K.; Kohno, T.; Ohtaka, H.; Kagaya, H.; Ito, K. *J. Med. Chem.* **1980**, *23*, 734.
(27) Piguet, C.; Bünzli, J. G.; Bernardinelli, G.; Hopfgartner, G.; Williams, A. F. *J. Am. Chem. Soc.* **1993**, *115*, 8197.
(28) Piguet, C.; Bocquet, B.; Hopfgartner, G.; *Helv. Chim. Acta* **1994**, *77*, 931.
(29) Kikugawa, Y. *Synthesis* **1981**, *2*, 124.
(30) Shao, C.; Sun, W.-H.; Li, Z.; Hu, Y.; Han, L. *Catal. Commun.* **2002**, *3*, 405.

Table 1. Selected Bond Lengths (Å) and Angles (deg) for Complexes 1b, 2a, 2b, and 5b (M = Co, Fe)

	1b	2b	2a	5b
		Bond Lengths		
M−N1	2.0197(1)	2.0003(2)	2.0989(2)	2.0627(2)
M−N2	2.0701(1)	2.0744 (2)	2.3322(2)	2.0912(2)
M−Cl1	2.2132(5)	2.2174(5)	2.3179(7)	2.2854(8)
M−Cl2/1A	2.2286(5)	2.2174(5)	2.3232(7)	2.2404(7)
N1−C1	1.392(2)	1.384(3)	1.392(3)	1.381(3)
N1−C7	1.327(2)	1.331(3)	1.327(3)	1.327(3)
N2−C8	1.358(2)	1.366(3)	1.358(3)	1.346(3)
N2−C12	1.347(2)	1.339(3)	1.334(3)	1.335(3)
C7−C8	1.468(2)	1.476(3)	1.472(3)	1.474(3)
M−O1			2.1702(2)	
		Bond Angles		
N2−M−N1	81.56(6)	80.56(7)	74.71(7)	77.36(8)
N2−M−Cl1	114.44(5)	115.05(3)	98.54(5)	104.18(6)
N1−M−Cl1	116.97(5)	117.13(3)	117.75(6)	106.55(6)
Cl1−M−Cl2/1A	111.27(2)	109.52(3)	125.07(3)	112.79(3)
N1−M−Cl2/1A	118.91(5)	117.13(3)	116.48(6)	106.08(6)
N2−M−Cl2/1A	110.27(4)	115.05(3)	87.46(5)	139.55(6)

of free organic compounds, the absorption bands of complexes were shifted to lower frequencies, indicating the coordination effects. The complexes are stable in their solid state; however, the color of the iron complex solutions slowly changed because of oxidation. To understand their real structures, the single crystals of complexes **1b**, **2a**,**b**, and **5b** were determined by single-crystal X-ray diffraction. Their molecular structures are discussed with their structural features, while their selected bond lengths and angles are collected in Table 1.

In the structure of **1b** (Figure 1), the geometry around the cobalt center can be described as a distorted tetrahedron, in which the cobalt was coordinated with the sp^2 N1 instead of sp^3 N3 in the benzimidazole ring. In this structure, the pyridine ring is almost coplanar with the benzimidazole ring (the dihedral angle is 2.3°). The $Co-N_{benzimidazole}$ bond length of 2.0197(1) Å is slightly shorter than the $Co-N_{pyridine}$ length of 2.0701(1) Å.

Single crystals of **2a** were obtained by diffusing a diethyl ether layer into its solution mixture of ethanol and DMF. The molecular structure of five-coordinated **2a** consists of a distorted-trigonal-bipyramidal geometry in which the iron atom is surrounded by one ligand, two chlorides, and one DMF molecule coordinated by an oxygen atom linkage (Figure 2). The axial positions are occupied by $N2_{pyridine}$ and O1 from the DMF molecule (N2−Fe1−O1 = 167.42(6)°), while the equatorial plane is formed by the nitrogen (N1) atom of benzimidazole and two chlorides with the deviation of the iron center from the equatorial plane by 0.1086 Å. The axial plane and the equatorial plane make a dihedral angle of 88.7°. The $Fe1-N2_{pyridine}$ bond (2.1702(2) Å) is significantly longer than the $Fe1-N1_{benzimidazole}$ bond (2.0989(2) Å), which can be attributed to the coordination of the DMF molecule. It is noteworthy that the benzimidazole ring and pyridyl ring are not coplanar, having a dihedral angle of 26.6°, which is different from the observation in complex **1b** and the following **2b** because of the different geometries around the metal center.

The molecular structure of **2b** showed the geometry of a distorted tetrahedron (Figure 3). In this structure, the $Co-N_{benzimidazole}$ bond length of 2.0003(2) Å is slightly shorter than the $Co-N_{pyridine}$ length of 2.0744(2) Å. However, different from the case for complex **1b**, **2b** displays an approximate C_s symmetry about the plane containing the cobalt atom and all the non-hydrogen atoms of **2**. The distortion from a regular tetrahedron is not as remarkable as that in the cobalt complexes which contain a steric substituent at the 6-position of the pyridine ring.[19c]

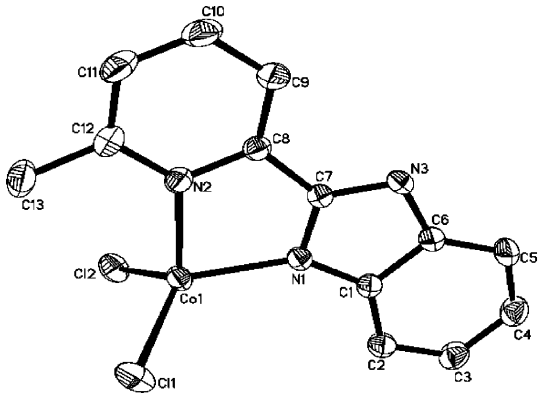

Figure 1. Molecular structure of **1b**. Thermal ellipsoids are shown at the 30% probability level. Hydrogen atoms have been omitted for clarity.

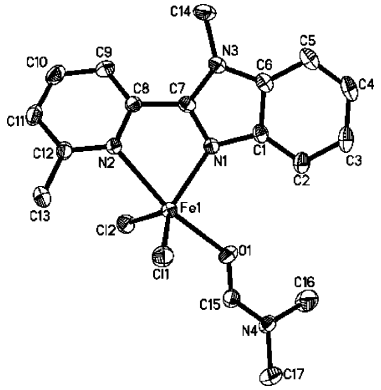

Figure 2. Molecular structure of **2a**. Thermal ellipsoids are shown at the 30% probability level. Hydrogen atoms have been omitted for clarity.

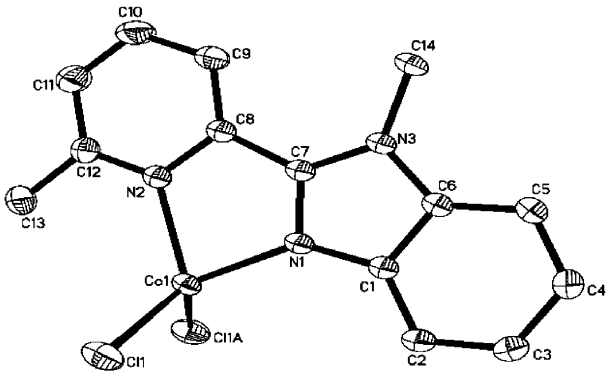

Figure 3. Molecular structure of **2b**. Thermal ellipsoids are shown at the 30% probability level. Hydrogen atoms have been omitted for clarity.

In the molecular structure of **5b** (Figure 4), the geometry around the cobalt center can be described as a distorted tetrahedron. The distance between the oxygen and cobalt atoms, Co1···O1, is 2.428 Å, which is substantially longer than the normal Co1−O1 bond distance (2.2191(2) Å).[31] The same observation was found in the (2-(ethylcarboxylato)-6-iminopyridyl)iron(II) and -cobalt(II) complexes, which indicated a weak interaction between the cobalt and carbonyl oxygen atoms.[18] In comparison with those in the cobalt complexes **1b** and **2b**, both the Co1−N1 and Co1−N2 bonds in **5b** are slightly longer, which can be attributed to the weak interaction between the

(31) March, R.; Clegg, W.; Coxall, R. A.; González-Duarte, P. *Inorg. Chim. Acta*, **2003**, *346*, 87.

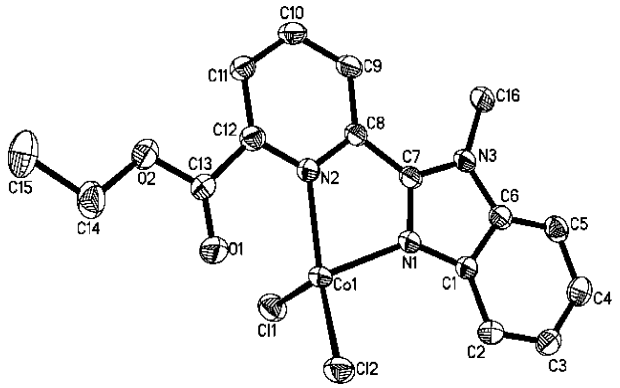

Figure 4. Molecular structure of **5b**. Thermal ellipsoids are shown at the 30% probability level. Hydrogen atoms have been omitted for clarity.

Scheme 3. Synthesis of 2-(1-Methyl-2-benzimidazolyl)-6-(1-(arylimino)ethyl)pyridines and Their Metal Complexes

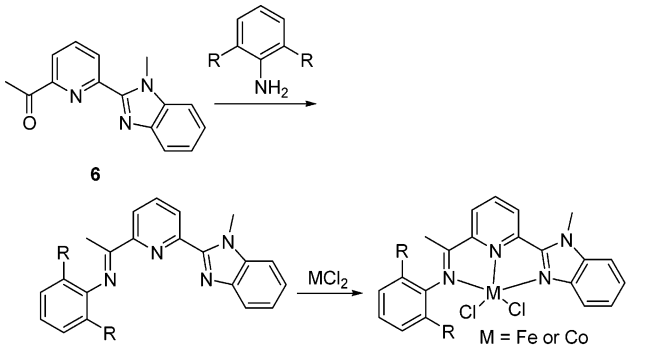

7: R = Me; **8**: R = Et; **9**: R = *i*-Pr; **10**: R = Cl; **11**: R = Br

	7a	8a	9a	10a	11a	7b	8b	9b	10b	11b
M	Fe	Fe	Fe	Fe	Fe	Co	Co	Co	Co	Co
R	Me	Et	*i*-Pr	Cl	Br	Me	Et	*i*-Pr	Cl	Br

cobalt and carbonyl oxygen atoms. The pyridine ring was nearly coplanar with the benzimidazole ring, having a dihedral angle of 5.1°.

2.3. Synthesis and Characterization of 2-(1-Methyl-2-benzimidazolyl)-6-(1-(arylimino)ethyl)pyridines (7−11) and Their Iron and Cobalt Complexes (7a−11a, 7b−11b). The 2-(1-methyl-2-benzimidazolyl)-6-(1-(arylimino)ethyl)pyridines **7**−**9** were easily prepared in satisfactory yields (68−89%) through the condensation reactions of 2-(1-methyl-2-benzimidazoleyl)-6-acetylpyridine ketones and the appropriate substituted anilines using *p*-toluenesulfonic acid as the catalyst;[32] however, the analogues **10** and **11** with halogen substituents on the phenyl ring were necessarily synthesized with a small amount of 4 Å molecular sieves as a water absorber (Scheme 3). The synthetic method with 4 Å molecular sieves as a water absorber offers the advantages of mild reaction conditions and smaller amount of solvent. The 2-(2-benzimidazolyl)-2-(1-(arylimino)ethyl) pyridines **7**−**11** were routinely characterized by elemental analysis and ^{1}H and ^{13}C NMR, IR, and ESI mass spectrometry. The IR spectra of the ligands showed that the C═N stretching frequencies appeared in the range of 1639−1650 cm^{-1}.

Their iron complexes **7a**−**11a** were prepared by stirring an ethanol solution of 1 equiv of $FeCl_2 \cdot 4H_2O$ and the corresponding ligands **7**−**11** at room temperature under nitrogen (Scheme 3). The obtained complexes were precipitated from the reaction solution and separated as blue powders in good yields (70−96%) with good purity. These complexes are air-stable in the solid state but turned from blue to yellow in solution when exposed to air for a few minutes, indicating their oxidation in solution. The formation of these complexes was confirmed by elemental analysis and IR. In comparison with the IR spectra of the free ligands with C═N stretching frequencies in the range of 1639−1650 cm^{-1}, the C═N stretching vibrations in complexes **7a**−**11a** were shifted toward lower frequencies in the range of 1591−1595 cm^{-1} with the reduced peak intensity, which indicated an effective coordination interaction between the imino nitrogen atom and the iron center.

By using the same synthetic method, the cobalt complexes **7b**−**11b** were conveniently prepared as green powders in isolated yields (46−73%) (Scheme 3). These cobalt complexes are stable in both solution and the solid state. Similar to the case for the iron analogues, all of the cobalt complexes showed lower frequencies of ν(C═N) with wavenumber shifts of 40−50 cm^{-1} along with a decreased peak intensity, in contrast to the signals for the corresponding free ligands.

Moreover, single crystals of **7** and **10** suitable for X-ray analysis were obtained by slow evaporation of their individual saturated ethyl acetate solutions. Single crystals of complexes **7a**, **10a**, **7b**, and **8b** were individually obtained by slow diffusion of diethyl ether into their methanol solutions under a nitrogen atmosphere, while single crystals of **10b** were obtained by the slow diffusion of diethyl ether into a saturated solution of the compound in methanol and DMF.

The crystal study of **7** and **10** revealed their *E* conformations as free molecules (Figure 4). The dihedral angles of the phenyl ring on imine with pyridine are 76.5° in **7** and 69.7° in **10**. Two planes of the benzimidazole and the pyridine are nearly coplanar with a dihedral angle of 0.2° in **7**; however, this phenomenon was not observed in **10**, in which the dihedral angle is 8.2°. The imino groups with a bond length of 1.2656(2) Å in **7** and 1.277(2) Å in **10** are in the range of typical C═N double-bond lengths. Their selected bond lengths and angles are listed below Figure 5.

An X-ray crystallographic study on the iron complex **7a** revealed the coordination geometry around metal center as a distorted trigonal bipyramid with the pyridyl nitrogen atom and the two chlorides forming an equatorial plane; the molecular structure is shown in Figure 6 with selected bond lengths and angles being given in Table 2. The deviation of the iron center from equatorial plane is 0.0075 Å, and the iron atom is nearly in this triangular plane with equatorial angles ranging between 133.00(1) and 115.68(1)°. The two nitrogen atoms (N1 and N3) occupy the axial coordination sites with a bond angle of 145.23(2)° for N1−Fe1−N3. The benzimidazole ring and the pyridyl ring are nearly coplanar, with a dihedral angle of 6.0°. The equatorial plane is oriented perpendicularly (86.6°) to the pyridine, and the dihedral angle between the phenyl ring and the pyridine is 83.3°. Nonetheless, the phenyl ring lies almost perpendicular to the plane formed by the coordinated nitrogen atoms (86.7°), which is similar to the case for the (2,6-bis(imino)pyridyl)iron(II) complexes[12,13] and (2-imino-1,10-phenanthrolinyl)iron(II) complexes.[21] Furthermore, the iron atom deviates by 0.2115 Å from this coordinated plane and the two Fe−Cl bond lengths show a slight difference between Fe−Cl1 (2.3131(1) Å) and Fe−Cl2 (2.2911(2) Å). The difference usually appears in tridentate N^N^N iron(II) complexes and may be ascribed to apical elongation in the square-pyramidal complex.[32b] The Fe−N2(pyridyl) (2.153(4) Å) bond is shorter (by about 0.13

(32) (a) Chen, Y.; Qian, C.; Sun, J. *Organometallics* **2003**, *22*, 1231. (b) Chen, Y.; Chen, R.; Qian, C.; Dong, X.; Sun, J. *Organometallics* **2003**, *22*, 4312.

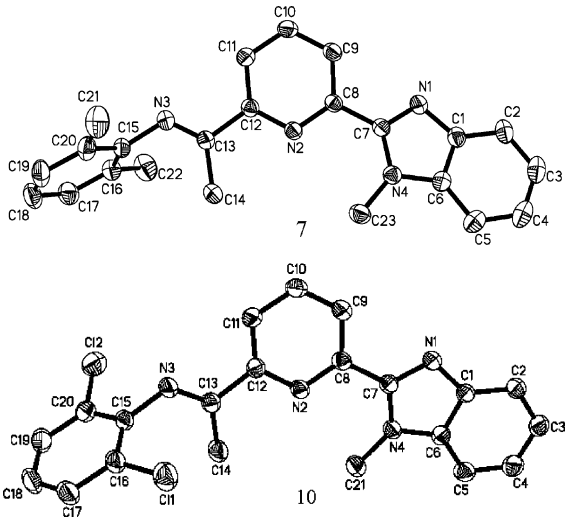

Figure 5. Molecular structures of **7** and **10**. Thermal ellipsoids are shown at the 30% probability level. Hydrogen atoms have been omitted for clarity. Selected bond distances (Å) and angles (deg) are as follows. **7**: N2−C8, 1.3372(2); N2−C12, 1.3387(2); N3−C13, 1.2656(2); N3−C15, 1.4237(2); N1−C7, 1.3189(2); N1−C1, 1.3798(2); C8−N2-C12, 118.04(1); C13−N3−C15, 121.16(1); C7−N1−C1, 104.67(1). **10**: N2−C8, 1.341(2); N2−C12, 1.348-(2); N3−C13, 1.277(2); N3−C15, 1.410(2); N1−C7, 1.319(2); N1−C1, 1.383(2); C8−N2−C12, 117.99(2); C13−N3−C15, 120.61(2); C7−N1−C1, 105.10(2).

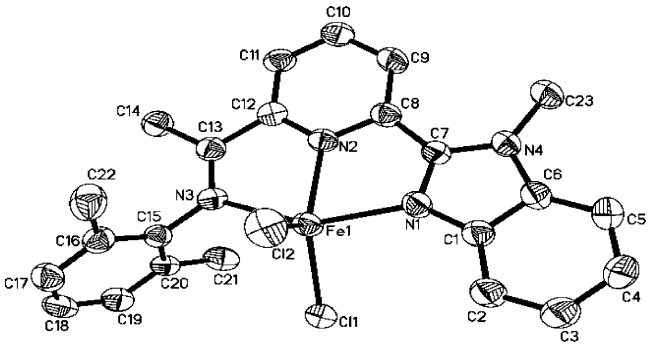

Figure 6. Molecular structure of **7a**. Thermal ellipsoids are shown at the 30% probability level. Hydrogen atoms and solvent molecules have been omitted for clarity.

Å) than the Fe−N3(imino) (2.283(4) Å) bond and is only slightly shorter than the Fe−N1(benzimidazole) (2.160(4) Å) bond. The imino N3−C13 bond in **7a** displays clear double-bond character (1.272(6) Å).

With structural features similar to those of **7a**, the molecular structure of complex **10a** is shown in Figure 7. According to Table 2, its Fe−N and Fe−Cl bond lengths are nearly the same as those of **7a**. In **10a**, the deviation of the iron center from the equatorial plane is 0.0678 Å. The two nitrogen atoms (N1 and N3) occupy the axial coordination sites with a bond angle of 142.45(8)° for N1−Fe1−N3. The equatorial plane is oriented perpendicularly (83.2°) to the pyridyl plane, and the dihedral angles between the phenyl ring and the pyridyl plane and between the phenyl ring and the benzimidazole plane are 86.7 and 92.1°, respectively. The phenyl ring also lies almost perpendicular to the plane formed by the coordinated nitrogen atoms. However, a slight difference exists between the two structures. The dihedral angle of the benzimidazole ring and the pyridyl ring is 9.5°, which is wider than that of complex **7a**. The deviation (0.4154 Å) of the iron atom from the coordinated plane is much greater than that observed in **7a**. These structural differences may be due to the different

Table 2. Selected Bond Lengths (Å) and Angles (deg) for Complexes 7a, 10a, 7b, 8b, and 10b (M = Co, Fe).

	7a	10a	7b	8b	10b
			Bond Lengths		
M−N1	2.160(4)	2.157(2)	2.1326(1)	2.132(2)	2.1293(2)
M−N2	2.153(4)	2.138(2)	2.0801(1)	2.079(2)	2.0889(1)
M−N3	2.283(4)	2.286(2)	2.2323(1)	2.209(2)	2.2661(2)
M−Cl1	2.3131(1)	2.2887(8)	2.2716(5)	2.2723(1)	2.2683(5)
M−Cl2	2.2911(2)	2.3197(8)	2.2790(5)	2.2643(1)	2.2978(5)
N1−C1	1.365(6)	1.383(3)	1.378(2)	1.384(4)	1.381(2)
N1−C7	1.316(6)	1.324(3)	1.329(2)	1.315(4)	1.326(2)
N2−C8	1.368(6)	1.354(3)	1.3462(2)	1.345(4)	1.342(2)
N2−C12	1.334(5)	1.328(3)	1.336(2)	1.333(4)	1.332(2)
N3−C13	1.272(6)	1.281(3)	1.280(2)	1.279(4)	1.278(2)
N3−C15	1.441(6)	1.429(3)	1.4400(2)	1.442(4)	1.427(2)
			Bond Angles		
N2−M−N1	73.95(2)	74.24(8)	75.95(5)	75.26(1)	75.65(6)
N2−M−N3	72.20(1)	71.65(8)	73.98(5)	74.12(9)	72.85(6)
N1−M−N3	145.23(2)	142.45(8)	147.76(5)	146.20(9)	144.46(6)
N2−M−Cl1	133.00(1)	147.68(6)	142.45(4)	98.34(8)	149.33(4)
N1−M−Cl1	97.55(1)	104.86(6)	98.31(4)	97.46(7)	102.17(4)
N3−M−Cl1	99.65(1)	95.81(6)	98.41(4)	100.80(8)	96.67(4)
Cl1−M−Cl2	111.32(6)	114.14(3)	115.71(2)	115.87(5)	113.93(2)
N1−M−Cl2	100.31(1)	96.92(6)	98.43(4)	98.16(7)	97.38(4)
N2−M−Cl2	115.68(1)	97.85(6)	101.83(4)	145.77(8)	96.58(4)
N3−M−Cl2	101.19(1)	102.79(6)	98.82(4)	99.07(8)	102.13(4)

electronic effects of chloro and methyl substituents. Similarly, the imino N3−C13 bond in **10a** displays clear double-bond character (1.281(3) Å) and is slightly longer than that of the free ligand **10**.

The cobalt analogues **7b**, with a 2,6-dimethylphenyl group, and **8b**, with a 2,6-diethylphenyl group, have the same structural character, as shown in Figure 8, along with the selected bond distances and angles given in Table 2. The coordination geometry around the cobalt center can be described as distorted trigonal bipyramidal, in which the nitrogen of the pyridyl group and two chlorides compose the equatorial plane, while the cobalt atom lies slightly out of the equatorial plane in **7b** (0.0110 Å) and **8b** (0.0143 Å). The axial planes are occupied by N1−Co1−N3, and the bond angles N1−Co1−N3 are nearly identical in the two complexes (147.76(5)° (**7b**) and 146.20(9)° (**8b**)). The equatorial planes of these two complexes are nearly perpendicular to the benzimidazole ring, with dihedral angles of 88.8° in **7b** and 88.3° in **8b**. The dihedral angles between the phenyl plane and the benzimidazole ring are 83.8° in **7b** and 85.6° in **8b**. The two imino C═N bonds have distinctive double-bond character, with C−N distances of 1.280(2) Å (**7b**) and 1.279-(4) Å (**8b**). The C═N bond in **7b** is about 0.015 Å longer than that of the corresponding free ligand, indicating coordination effects in the iron analogues. The steric effect of the substituents at the ortho positions of the phenyl ring are slightly reflected in the adjacent bond lengths. The Co1−N(imino) bond length of **7b** (2.2323(1) Å) is noticeably longer than that of **8b** (2.209-(2) Å). This effect is due to the relatively bulkier ethyl groups at the ortho positions of the phenyl ring in **8b**.

The molecular structure of complex **10b** is shown in Figure 9. The cobalt atom slightly deviates by 0.0458 Å from the equatorial plane. The three equatorial angles N2−Co1−Cl1, N2−Co1−Cl2, and Cl1−Co1−Cl2 are 149.33(4), 96.58(4), and 113.93(2)°, respectively, while the larger distortion of N2−Co1−Cl1 and the axial Co1−N bonds subtend an angle of N1−Co1−N3 (144.46(6)°). The dihedral angle between the equatorial plane and the benzimidazole plane is 84.2°, while the dihedral angle between the phenyl plane and the benzimidazole plane is 93.0°. Its two axial Co1−N bond lengths (2.1293(2) and 2.2661(2) Å) are longer than Co1−N2 in the equatorial plane (2.0889(1) Å), which is usually observed in (bis(imino)-

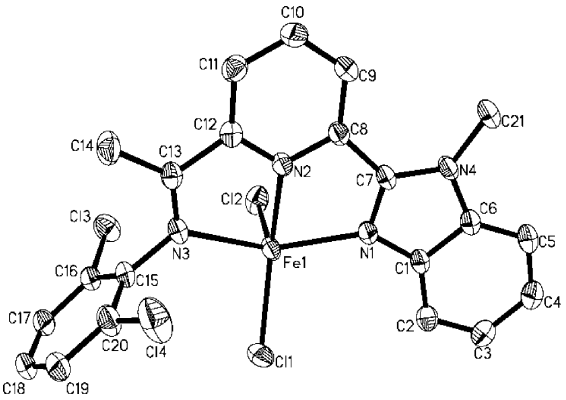

Figure 7. Molecular structure of **10a**. Thermal ellipsoids are shown at the 30% probability level. Hydrogen atoms have been omitted for clarity.

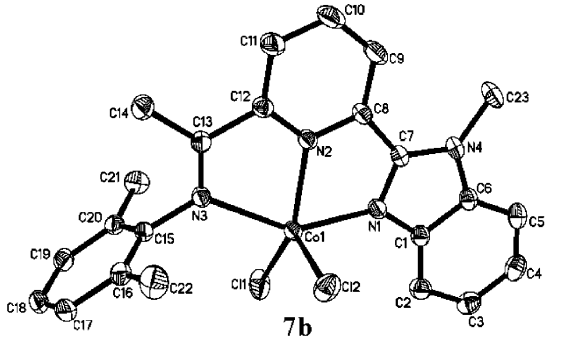

7b

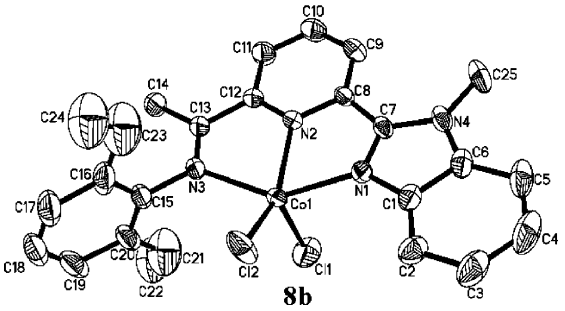

8b

Figure 8. Molecular structures of **7b** and **8b**. Thermal ellipsoids are shown at the 30% probability level. Hydrogen atoms have been omitted for clarity.

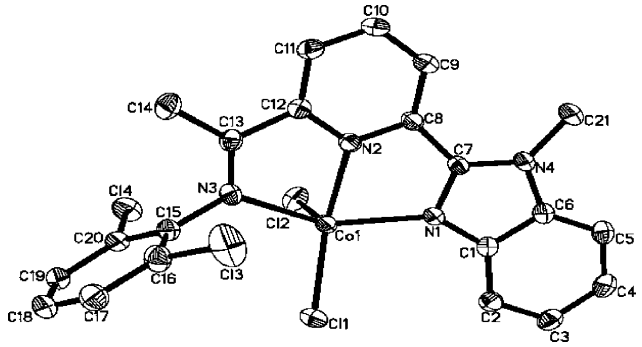

Figure 9. Molecular structure of **10b.** Thermal ellipsoids are shown at the 30% probability level. Hydrogen atoms have been omitted for clarity.

pyridyl)cobalt(II) complexes.[12,13] In comparison with the 2,6-dialkylphenyl complexes **7b** and **8b**, Co1−N1 and Co1−N2 have almost identical bond lengths, while the Co1−N3(imino) bond length of **10b** is relatively longer than that of **7b** and **8b**. The imino N3−C13 bond length is 1.278(2) Å, having the typical character of a C═N double bond. These facts suggest that the introduction of electron-withdrawing substituents on the phenyl rings slightly affects the structural properties. Moreover, the difference between the two Co1−Cl linkages, Co1−Cl2 (2.2978(5) Å) and Co1−Cl1 (2.2683(5) Å), is about 0.03 Å.

Table 3. Ethylene Oligomerization by Metal Complexes Ligated with 1, 2 and 4−6 and Their Oligomer Distribution[a]

					oligomer distribn (%)[c]	
entry	cat.	cocat.	Al/M	activity[b]	$C_4/\sum C$	$C_6/\sum C$
1	**1a**	MMAO	1000	0.86	81.4	18.6
2	**1a**	Et_2AlCl	500	0.56	58.7	41.3
3	**1a**	Et_2AlCl	200	0.38	60.2	39.8
4	**1a**	MAO	1000	0.26	53.9	46.1
5	**2a**	MMAO	1000	0.78	68.3	31.7
6	**4a**	MMAO	1000	5.15	96.3	3.4
7	**5a**	MMAO	1000	3.33	96.3	3.7
8	**6a**	MMAO	1000	0.90	75.0	25.0
9	**6a**	Et_2AlCl	200	1.29	76.2	23.8
10	**1b**	Et_2AlCl	500	1.29	67.4	32.6
11	**1b**	Et_2AlCl	200	1.41	70.5	29.5
12	**2b**	Et_2AlCl	200	0.80	37.4	62.6
13	**4b**	Et_2AlCl	200	1.13	81.6	18.4
14	**5b**	Et_2AlCl	200	0.76	77.9	22.1
15	**6b**	Et_2AlCl	200	0.80	48.5	51.5

[a] Conditions: 5 μmol of catalyst; 30 min; 20 atm of ethylene, 20 °C, 100 mL of toluene. [b] In units of 10^4 g (mol of M)$^{-1}$ h^{-1} atm^{-1}. [c] Determined by GC; $\sum C$ signifies the total amounts of oligomers.

2.4. Ethylene Oligomerization and Polymerization. 2.4.1. Ethylene Oligomerization by Bidentate Metal Complexes. Different functional groups and coordinated environments of the complexes affected their catalytic behaviors toward ethylene activation. Prior to investigating the titled complexes, the metal complexes bearing bidentate N^N coordinated ligands of various 6-substituted 2-benzimidazolylpyridines such as **1**, **2**, and **4**−**6** were also synthesized and investigated for their ethylene oligomerzation. When different organoaluminum were used at an ambient pressure of ethylene, these iron and cobalt complexes showed very low catalytic activities; therefore, 20 atm of ethylene was fixed for the reaction. Considerable catalytic activities of iron complexes were obtained with cocatalysts such as MAO, MMAO, and Et_2AlCl. As a matter of fact, in general, the catalytic system with MAO showed activities lower than those with MMAO or Et_2AlCl on the basis of the results of **1a** (Table 3). However, their cobalt analogues showed low activities toward ethylene reactivity with cocatalysts of MAO and MMAO but good activities with Et_2AlCl (Table 3).

In comparison with the metal complexes ligated by **2** as catalysts (entries 5 and 12 in Table 3), the catalytic systems of complexes **1a**,**b** had relatively higher activities (entries 1 and 11 in Table 3), and the same tendency was also observed in the complexes ligated by **4** and **5** (entry 6 vs 7 and entry 13 vs 14 in Table 3). These results, which concurred with the literature reports,[24,33] can be attributed to the deprotonation of the N−H group to give anionic amide ligands and form N−Al species to increase their catalytic activity when activated by the organoaluminum cocatalyst. The iron complexes **4a** and **5a**, containing a carboxylate group at the 6-position of the pyridine ring, exhibited reactivities higher than those of their analogues ligated by **1** and **2**, even better than those containing **6**. This phenomenon could be assumed to be the result of the better solubility of complexes or the electron-withdrawing effect of the carboxylate group and the weak metal−oxygen interaction.[19c] Furthermore, when iron complexes with an ester group were

(33) McGuinness, D. S.; Wasserscheid, P.; Morgan, D. H.; Dixon, J. T. *Organometallics* **2005**, *24*, 552.

Table 4. Ethylene Oligomerization of the 6a/Et_2AlCl System[a]

					oligomer distribn (%)[c]	
entry	Al/Fe	*P*/atm	*T*/°C	activity[b]	$C_4/\sum C$	$C_6/\sum C$
1	50	20	20	0.54	33.8	66.2
2	100	20	20	1.03	66.2	33.8
3	200	20	20	1.29	76.2	23.8
4	300	20	20	1.07	60.0	40.0
5	500	20	20	1.00	64.8	35.2
6	200	10	20	1.43	73.4	26.6
7	200	30	20	1.01	75.0	25.0
8	200	20	40	2.40	86.3	13.7
9	200	20	60	0.91	72.6	27.4
10	200	20	80	0.48	47.7	52.3

[a] Conditions: 5 μmol of catalyst; 30 min; 100 mL of toluene. [b] In units of 10^4 g (mol of M)$^{-1}$ h^{-1} atm^{-1}. [c] Determined by GC; $\sum C$ signifies the total amounts of oligomers.

used as the catalysts, the C_6 proportion in the products was much lower than that for the other catalytic systems; the possible reason for this could be the occurrence of faster elimination. Nevertheless, the catalytic activities of the cobalt complexes were hardly different with different substituents on the pyridyl group. This indicates that different coordination environments for cobalt complexes in benzimidazole derivatives exhibit little influence on ethylene activation. In general, the cobalt complexes generally exhibited activities 1 order of magnitude lower than those of the iron analogues. In comparison with similar catalytic systems of complexes bearing acetyliminopyridine[34] and 2-(ethylcarboxylato)-6-iminopyridine ligands,[19g] the catalysts in this work gave oligomers with shorter carbon chains (C_4 and C_6).

Varying catalytic conditions such as the reaction temperature and pressure of ethylene were also investigated. Since comparable catalytic activities by cocatalysts of MMAO and Et_2AlCl were observed, Et_2AlCl was selected in the catalytic system of **6a**, which also avoided the effect of MMAO on the contribution of C_4 in their products (Table 4). According to the data in Table 4, the optimum catalytic activity was obtained in the system with an Al/Fe molar ratio of 200. Both increasing and decreasing the Al/Fe molar ratio led to lower activity (entries 1−5 in Table 4). No obvious change in catalytic activities was observed by elevating the ethylene pressure from 10 to 30 atm (entries 3, 6, and 7 in Table 4). In addition, the highest activity was obtained at 40 °C; higher reaction temperatures resulted in a sharp decrease in activity (entries 8−10 in Table 4), which can be explained by the decomposition of reactive species and lower ethylene solubility at higher temperature.[35] Additionally, for the above catalytic reactions, C_4 and C_6 were produced as the main products and no wax was obtained.

2.4.2. Ethylene Reactivity Catalyzed by the Tridentate Iron Complexes. Generally, the catalytic activities of the title tridentate complexes were scanned in the presence of various cocatalysts such as MAO, MMAO, and Et_2AlCl, and the catalytic systems with MAO or MMAO had high activity and were worthy of careful investigation. It has commonly been observed that the catalytic behaviors of iron and cobalt complexes toward ethylene oligomerization and polymerization are similar; however, in our investigation, there are some differences in their catalytic activities. Therefore, the discussion of their reactivity with ethylene is separated into two parts.

Table 5. Selection of a Suitable Cocatalyst Based on 7a[a]

entry	cocat.	Al/Fe	oligomer activity[b]	oligomer distribn	polymer activity[b]
1	MAO	1000	9.2	C_4-C_{28}	1.0
2	MMAO	1000	12.0	C_4-C_{26}	trace
3	Et_2AlCl	200			

[a] Reaction conditions: 5 μmol of **7a**, 10 atm of ethylene; 30 min; 20 °C; 100 mL of toluene. [b] In units of 10^4 g (mol of Fe)$^{-1}$ h^{-1} atm^{-1}.

2.4.2.1. Catalytic Behavior of the Tridentate Iron Complexes. Cocatalyst Selection. The catalytic activities of iron(II) complexes for ethylene activation were evaluated in the presence of different cocatalysts such as methylaluminoxane (MAO), modified methylaluminoxane (MMAO), and Et_2AlCl. Because of the low catalytic activity at ambient pressure of ethylene, it is hard to evaluate the effect of the cocatalyst. An elevated pressure of ethylene (10 atm) was used, and the effects of cocatalysts were studied in detail with **7a** (Table 5). The results showed that MAO and MMAO could be promising cocatalysts for ethylene activation.

2.4.2.2. Ethylene Activation in the Presence of MAO. After routine selection of the ratio of MAO to iron catalyst, good catalytic activity was observed at an Al/Fe molar ratio of 1000. Therefore, the catalytic behaviors of all tridentate iron complexes were investigated with a fixed Al/Fe molar ratio of 1000, and their resultant data are summarized in Table 6. All of the complexes displayed high catalytic activities for ethylene oligomerization with high α-olefin selectivity (>99%) at 30 atm of ethylene pressure. The distribution of obtained oligomers resembled Schulz−Flory rules, and the probability of chain propagation is represented with the constant *K*, where *K* = rate of propagation/((rate of propagation) + (rate of chain transfer)) = (moles of C_{n+2})/(moles of C_n); the *K* values are determined by the molar ratio of C_{12} and C_{14} fractions.[36] The distribution of the oligomers (entries 4−6 of Table 6) are shown in detail in Figure 10.

As depicted in Table 6, the higher the ethylene pressure, the higher the catalytic activity. The ethylene concentration significantly affected the catalytic behaviors. At ambient ethylene pressure, only C_4 and C_6 were produced; the higher pressure, however, increased the chain propagation, leading to longer chain oligomers up to the range of C_4-C_{28} in addition to the improved activity. At 30 atm, all iron complexes had high activity toward ethylene oligomerization with some amount of polyethylene waxes produced.

The steric effect of ligands on the activities of iron complexes is easily observed. As indicated by entry 6 of Table 6, **9a**, containing 2,6-diisopropyl substituents, showed the highest oligomerization activity at 47.7×10^4 g (mol of Fe)$^{-1}$ h^{-1} atm^{-1}. This could be explained by the less bulky substituents rendering the active sites of the catalyst exposed to not only ethylene but also other reactive species, and the latter actually lead to the deactivation of the active species. Indeed, Gibson has proved that the catalytic intermediates formed from precursors containing pyridyldiimine ligands are more easily deactivated through the interaction with alkylaluminum reagent if they lack sufficient steric bulk in the aryl ring.[35b] Meanwhile, with higher catalytic activity, the content of C_4 is obviously increased, and the distribution of obtained oligomers did not resemble Schulz−Flory rules (entries 5 and 6 in Table 6). The electronic effect of ligands on the activities of iron complexes was also

(34) Bluhm, M. E.; Folli, C.; Döring, M. *J. Mol. Catal. A* **2004**, *212*, 13.

(35) (a) Britovsek, G. J. P.; Bruce, M.; Gibson, V. C.; Kimberley, B. S.; Maddox, P. J.; Mastroianni, S.; McTavish, S. J.; Redshaw, C.; Solan, G. A.; Strömberg, S.; White, A. J. P.; Williams, D. J. *J. Am. Chem. Soc.* **1999**, *121*, 8728. (b) Britovsek, G. J. P.; Mastroianni, S.; Solan, G. A.; Baugh, S. P. D.; Redshaw, C.; Gibson, V. C.; White, A. J. P.; Williams, D. J.; Elsegood, M. R. J. *Chem. Eur. J.* **2000**, *6*, 2221.

(36) (a) Schulz, G. V. *Z. Phys. Chem., Abt. B* **1935**, *30*, 379. (b) Schulz, G. V. *Z. Phys. Chem., Abt. B* **1939**, *43*, 25. (c) Flory, P. J. *J. Am. Chem. Soc.* **1940**, *62*, 1561. (d) Henrici-Olivé, G.; Olivé, S. *Adv. Polym. Sci.* **1974**, *15*, 1.

Table 6. Polymerization and Oligomerization of Ethylene with 7a−11a/MAO[a]

					activity[b]		oligomer distribn (%)[c]				
entry	cat.	*P*/atm	K	amt of wax/g	oligomer	wax	$C_4/\sum C$	$C_6/\sum C$	$C_8/\sum C$	$C_{10}/\sum C$	$C_{\geq 12}/\sum C$
1	**7a**	1			3.10		83.7	16.3			
2	**9a**	1			3.50		95.0	5.0			
3	**7a**	10	0.65	0.25	9.20	1.00	20.0	17.3	13.8	10.5	38.4
4	**7a**	30	0.58	0.67	22.2	0.90	26.0	21.2	17.7	10.9	24.0
5	**8a**	30	0.58	1.02	24.6	1.37	41.7	23.6	13.0	8.1	13.6
6	**9a**	30	0.58	0.77	47.7	1.03	42.3	24.8	12.7	7.0	13.2
7	**10a**	30	0.48		1.07	trace	37.3	25.8	14.2	8.9	13.6
8	**11a**	30	0.46		3.87	trace	32.3	21.2	14.7	9.9	21.9

[a] Reaction conditions: 5 μmol of catalyst; Al/Fe = 1000; 30 atm of ethylene; 30 min; 20 °C, 100 mL of toluene. [b] In units of 10^4 g (mol of Fe)$^{-1}$ h^{-1} atm^{-1}. [c] Determined by GC; $\sum C$ signifies the total amounts of oligomers.

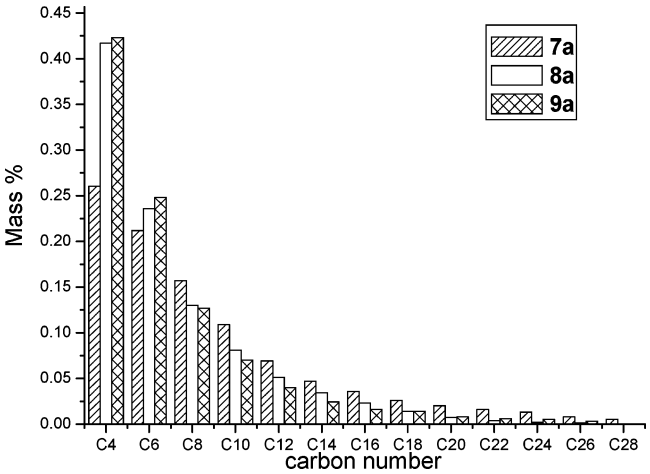

Figure 10. Oligomer distribution obtained in entries 4−6 in Table 6.

considered. Complexes **10a** and **11a**, bearing halogen groups, exhibited lower activity than complexes bearing alkyl groups (entries 4−8 in Table 6). Furthermore, the bromo-substituted complex **11a** showed much higher oligomerization activity than **10a**, which can be explained as the total result of the electronic and steric effects and the influence of the reaction between the halogen substituent catalyst and the Lewis acidic activators. It is noteworthy that only trace waxes were produced by the complexes with electron-withdrawing groups. Therefore, bulky ligands with electron-donating substituents would be helpful in increasing the catalytic activity of the tridentate iron complexes in the presence of MAO.

2.4.2.3. Ethylene Activation in the Presence of MMAO. In the presence of MMAO as cocatalyst, the tridentate iron complexes were carefully investigated under various reaction conditions, including changing the ethylene pressure, molar ratio of MMAO to iron, and reaction temperature. In a pattern similar to that with MAO, the oligomers range from C_4 to C_{28} with high selectivity for α-olefins (>99%), and the results are given in Table 7 (K = (moles of C_{n+2})/(moles of C_n) and is determined by the molar ratio of C_{12} and C_{14} fractions[36]).

Guided by the experience of the catalytic system with MAO, the various Al/Fe molar ratios were studied with **7a** at 30 atm of ethylene. When the Al/Fe molar ratio was varied from 200 to 1500, the catalytic activities for both oligomers and polyethylene waxes initially increased and then decreased (entries 1−4 in Table 7). Notably, the catalytic activity increased sharply from 200 to 500, which may be attributed to the fact that MMAO scavenged adventitious water and impurities in the solvent at an Al/Fe ratio of 200 and the iron catalysts require more cocatalyst to be active. At an Al/Fe ratio of 1000, the catalytic activities for both ethylene oligomerization and polymerization were attained at the highest value. Increasing the Al/Fe molar ratio to 1500 led to lower activity. This observation could be traced to the increasing amount of isobutyl groups, and the generated species hinder the insertion reaction of ethylene due to steric bulkiness.[37]

To ascertain the relationship between catalytic activity and ethylene pressure, the catalytic system of **7a** with 1000 equiv of MMAO at room temperature was investigated by varying the ethylene pressure (entries 3, 5, and 6 in Table 7). The phenomena were found to be the same as those with MAO as cocatalyst. The higher the ethylene pressure, the higher the catalytic activity. It is also worth mentioning that the ethylene pressure affects the distribution of oligomers (Figure 11). This point could be considerably useful in future industrial processes, and the distribution of oligomers will be slightly changed with changing ethylene pressure.

As the ethylene oligomerization and polymerization are highly exothermic reactions, the reaction temperature significantly affects the catalytic activity. To understand this influence, the catalytic system of **7a** with 1000 equiv of MMAO at 30 atm of ethylene was investigated with changing reaction temperature (entries 3, 11, and 12 in Table 7). Elevation of the reaction temperature from 20 to 60 °C resulted in a sharp decrease of catalytic activity, which can be explained as catalyst decomposition and lower ethylene solubility at higher temperature.[35] Moreover, the oligomer distribution became narrower, along with a decreased reactivity. The proportion of C_4 and other short-chain oligomers was greatly increased at higher temperature because β-hydrogen elimination was faster than ethylene propagation and the distribution of obtained oligomers did not resemble Schulz−Flory rules (entries 11 and 12 in Table 7).

The natural catalytic behaviors of these tridentate iron complexes with MMAO are rooted in their ligands with different substituents. In the presence of MMAO as cocatalyst, complexes **7a**−**11a** also showed high activities for ethylene oligomerization along with moderate activities for ethylene polymerization (entries 3 and 7−10 in Table 7). On the basis of these data, their oligomerization activity varied in the order of **9a** (with an *i*-Pr substituent) < **8a** (with Et) < **7a** (with Me) and **11a** (with Br) < **10a** (with Cl), and this order was reversed in catalytic systems with MAO as cocatalyst. In the catalytic system with MMAO, it is assumed that the factor controlling the reaction speed mostly relies on the insertion of ethylene at the active metal center, and a more bulky group causes a slower insertion reaction and consequently lower activity. This observation could be traced to the isobutyl group, and therefore, the generated species hinder the insertion reaction of ethylene due to steric

(37) (a) Chen, E. Y.; Marks, T. J. *Chem. Rev.* **2000**, *100*, 1391. (b) Karam, A. R.; Catarí, E. L.; López-Linares, F.; Agrifoglio, G.; Albano, C. L.; Díaz-Barrios, A.; Lehmann, T. E.; Pekerar, S. V.; Albornoz, L. A.; Atencio, R.; González, T.; Ortega, H. B.; Joskowics, P. *Appl. Catal. A: Gen.* **2005**, *280*, 165.

Table 7. Polymerization and Oligomerization of Ethylene with 7a−11a/MMAO[a]

							activity[b]		oligomer distribn (%)[c]				
entry	cat.	Al/Fe	*P*/atm	K	*T*/°C	amt of wax/g	oligomer	wax	$C_4/\sum C$	$C_6/\sum C$	$C_8/\sum C$	$C_{10}/\sum C$	$\sum C_{\geq 12}/\sum C$
1	**7a**	200	30	0.52	20	0.08	0.60	0.10	46.1	22.1	11.5	6.5	13.8
2	**7a**	500	30	0.44	20	0.10	19.0	0.13	35.7	28.7	16.7	8.7	10.2
3	**7a**	1000	30	0.53	20	0.90	26.4	1.20	35.0	27.8	15.2	8.1	13.9
4	**7a**	1500	30	0.54	20	0.25	7.57	0.33	37.3	24.7	14.6	8.9	14.5
5	**7a**	1000	10	0.62	20		12.0	trace	38.5	14.9	11.6	9.3	25.7
6	**7a**	1000	20	0.59	20	0.05	8.20	0.10	42.5	21.0	13.7	8.2	14.6
7	**8a**	1000	30	0.55	20	0.32	22.3	0.43	26.3	22.5	18.0	12.4	20.8
8	**9a**	1000	30	0.51	20	0.85	4.67	1.13	59.6	21.3	9.1	3.9	6.1
9	**10a**	1000	30	0.56	20		12.9	trace	28.2	26.4	18.5	11.1	15.8
10	**11a**	1000	30	0.52	20		7.07	trace	46.9	26.1	11.8	6.1	9.1
11	**7a**	1000	30	0.47	40		0.77	trace	65.5	16.3	8.7	5.0	4.5
12	**7a**	1000	30	0.57	60		0.50	trace	68.0	18.9	6.1	4.2	3.0
13[d]	**7a**	1000	30	0.45	20		2.20	trace	47.3	20.8	14.4	7.1	10.3

[a] Reaction conditions: 5 μmol of catalyst; 30 min; 100 mL of toluene. [b] In units of 10^4 g (mol of Fe)$^{-1}$ h^{-1} atm^{-1}. [c] Determined by GC; $\sum C$ signifies the total amounts of oligomers. [d] Five equivalents of PPh_3.

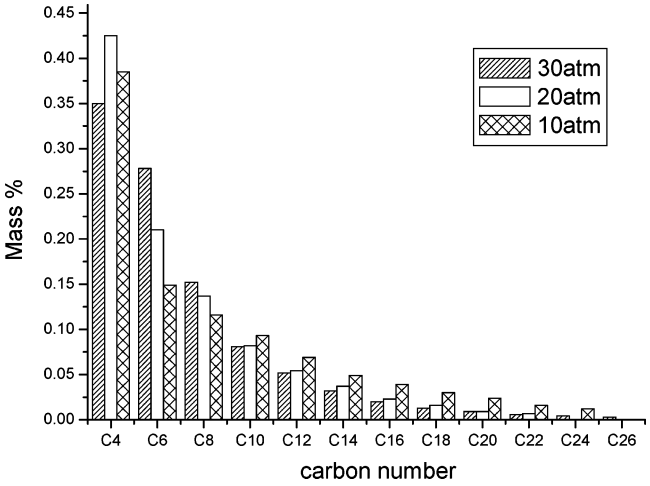

Figure 11. Oligomer distribution obtained in entries 3, 5, and 6 in Table 7.

bulkiness.[37] Complex **10a**, with a dichloro-substituted ligand, displayed ethylene oligomerization activity higher than that of its analogue **11a**, containing a dibromo-substituted ligand. Similar to the case for the catalytic system with MAO, the distribution of obtained oligomers did not resemble Schulz−Flory rules with a sterically large, bulky group on the N-aryl ring (entries 8 and 10 in Table 7).

Previous studies reported that nickel-based catalysts incorporated PPh_3 in catalytic systems, resulting in higher activity and longer catalyst lifetime.[22a,23a,38] Therefore, the oligomerization reaction with the **7a**/MMAO system was carried out in the presence of 5 equiv of PPh_3 (entry 13 of Table 7). However, a sharp decrease in catalyst activity was observed and no polyethylene waxes were produced. This can be explained by the fact that the stronger Fe−P bond prevented the insertion of ethylene at the active metal center.

2.4.2.4. Characterization of Low-Molecular-Weight Waxes. In addition to high selectivity for α-olefins, polyethylene waxes were also obtained in some catalytic systems. As characterized by IR spectra recorded using KBr disks in the range of 4000−400 cm^{-1}, the polyethylene waxes were confirmed to be highly linear α-olefins, from the characteristic vibration absorption bands of various C−H and C═C bonds. ^{1}H and ^{13}C NMR spectra of the polyethylene waxes obtained by **8a**/MAO were recorded at 110 °C in *o*-dichlorobenzene-d_4 using TMS as the internal standard. NMR spectra are shown in Figure 12, and the assignments were determined according to the literature.[39] The ^{13}C NMR spectra further demonstrated that linear α-olefins of the waxes absolutely predominated in the polymers, and the single peaks at δ 140.0 and 115.1 ppm showed the property of a vinyl-unsaturated chain end. The obtained average molecular weight from ^{13}C NMR indicated that the carbon number of the polymeric waxes is about 60. Other ethylene waxes showed very similar NMR spectra, to confirm the linear α-olefin fashion of polymeric alkenes.

To briefly summarize, cocatalysts of both MAO and MMAO could activate the tridentate iron complexes to be highly active toward ethylene activation. The selectivity of forming α-olefins is generally very high; even the ethylene waxes showed high selectivity to be vinyl-terminal long-chain alkenes. However, the catalytic activities of MAO and MMAO are quite different, especially with regard to the bulky effect of substituents in their ligands, such as that caused by a bulky isobutyl group in MMAO.

2.4.3. Ethylene Oligomerization by Tridentate Cobalt Complexes. Similar to the case for the iron complexes above, all of the cobalt(II) analogues displayed moderate catalytic activities for ethylene oligomerization with high selectivity for α-olefins (>98%) at 30 atm of ethylene pressure in the presence of MAO (Table 8). Though MMAO or Et_2AlCl could also be used as the cocatalyst, these catalytic systems yielded lower catalytic activities (entries 6 and 7 in Table 8). Therefore, further detailed investigation was carried out using MAO as the cocatalyst. The obtained oligomers were only C_4 and C_6 without polymeric products. As reported in previous studies, the cobalt catalyst system displayed activities that are an order of magnitude lower than that of their iron analogues.[32,35b,40]

The catalytic activities of cobalt complexes are significantly affected by their ligands' environment. As shown in Table 8, the ethylene oligomerization activity varied in the order **7b** > **8b** > **9b** and **10b** > **11b**. The catalysts bearing less bulky substituents displayed higher activity than those with sterically bulky substituents. This can perhaps be attributed to a weaker interaction between the cobalt atom and the π-electrons of the

(38) (a) Carlini, C.; Isola, M.; Liuzzo, V.; Galletti, A. M. R.; Sbrana, G. *Appl. Catal. A: Gen.* **2002**, *231*, 307. (b) Jenkins, J. C.; Brookhart, M. *Organometallics* **2003**, *22*, 250. (c) Sun, W.-H.; Zhang, W.; Gao, T.; Tang, X.; Chen, L.; Li, Y.; Jin, X. *J. Organomet. Chem.* **2004**, *689*, 917. (d) Tang, X.; Zhang, D.; Jie, S.; Sun, W.-H.; Chen, J. *J. Organomet. Chem.* **2005**, *690*, 3918.

(39) (a) Kokko, E.; Lehmus, P.; Leino, R.; Luttikhedde, H. J. G.; Ekholm, P.; Näsman, J. H.; Seppälä, J. V. *Macromolecules* **2000**, *33*, 9200. (b) Galland, G. B.; Quijada, R.; Rojas, R.; Bazan, G.; Komon, Z. J. A. *Macromolecules* **2002**, *35*, 339.

(40) Bianchini, C.; Mantovani, G.; Meli, A.; Migliacci, F.; Zanobini, F.; Laschi, F.; Sommazzi, A. *Eur. J. Inorg. Chem.* **2003**, *8*, 1620.

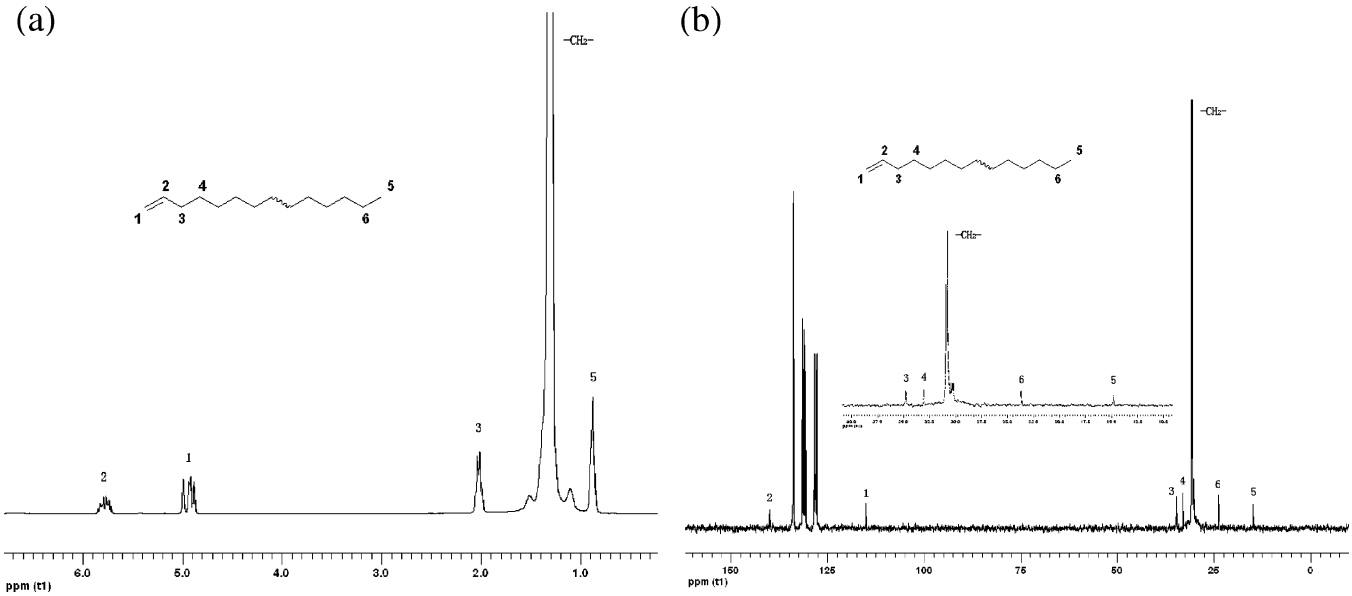

Figure 12. ^{1}H NMR (a) and ^{13}C NMR (b) spectra of the waxes obtained by complex **8a** in entry 5 in Table 6.

Table 8. Oligomerization of Ethylene by 7b−11b[a]

							oligomer distribn (%)[c]	
entry	cat.	cocat.	Al/Co	*P*/ atm	*T*/ °C	activity[b]	$C_4/\Sigma C$	$C_6/\Sigma C$
1	**7b**	MAO	1000	1	20	0.88	100	
2	**9b**	MAO	1000	1	20	0.82	100	
3	**7b**	MAO	1000	10	20	1.40	100	
4	**7b**	MAO	1000	20	20	1.58	77.8	22.2
5	**7b**	MAO	1000	30	20	11.8	90.0	10.0
6	**7b**	MMAO	1000	30	20	2.37	85.0	15.0
7	**7b**	Et_2AlCl	200	30	20	2.33	85.0	15.0
8	**8b**	MAO	1000	30	20	8.60	94.6	5.40
9	**9b**	MAO	1000	30	20	4.67	89.3	10.7
10	**10b**	MAO	1000	30	20	2.80	83.3	16.7
11	**11b**	MAO	1000	30	20	1.87	75.8	24.2
12	**7b**	MAO	1500	30	20	4.67	88.6	11.4
13	**7b**	MAO	500	30	20	2.10	74.7	25.3
14	**7b**	MAO	1000	30	40	3.00	70.6	29.4
15	**7b**	MAO	1000	30	60	2.37	91.5	8.50

[a] Reaction conditions: 5 μmol of catalyst; 30 min; 100 mL of toluene. [b] In units of 10^3 g (mol of Co)$^{-1}$ h^{-1} atm^{-1}. [c] Determined by GC; ΣC signifies the total amounts of oligomers.

ethylene monomer, due to bulkier groups on the phenyl ring, which resulted in a decrease in the rate of ethylene insertion in the chain-growth steps. For **10b** and **11b**, as a consequence of electronegativity Cl > Br; **10b** displayed higher reactivity than **11b** when the central metal positive charge was increased.

When reaction parameters were varied, the catalytic activities of cobalt complexes were also affected. When the Al/Co molar ratio was increased from 500 to 1500, the catalytic activities initially increased and then decreased, with the optimum activity being at an Al/Co molar ratio of 1000 (entries 5, 12, and 13 in Table 8). Elevating the reaction temperature from 20 to 60 °C resulted in decreasing catalytic activity (entries 5, 14, and 15 in Table 8), which might be caused by instability of the active species or a lower concentration of ethylene in the reaction solution. Commonly, a lower catalytic activity was observed at lower pressure and only butenes were produced at an ethylene pressure lower than 10 atm (entries 1 and 3−5 in Table 8).

3. Conclusion

Inspired by the success of bis(imino)pyridyliron dihalide[12,13] and 2-imino-1,10-phenanthrolyliron dihalide[21,23] as highly active catalysts toward ethylene activation, 2-(benzimidazolyl)-6-(1-(arylimino)ethyl)pyridines have been successively synthesized and used to form their iron and cobalt complexes. In the presence of either MAO or MMAO, the tridentate iron complexes had very high catalytic activities, up to 47.7×10^4 g (mol of^{-1}Fe)$^{-1}$ h^{-1} atm^{-1}, in producing α−olefins (C_4−C_{28}) with high selectivity. The tridentate cobalt complexes showed moderate activities when activated by MAO cocatalysts. In synthesizing 2-(benzimidazolyl)-6-(1-(arylimino)ethyl)pyridines, the intermediates of 2-(benzimidazolyl)-6-substituted-pyridines could be used as bidentate ligands to form their iron and cobalt complexes. The bidentate metal complexes could provide moderate to good catalytic activities toward ethylene oligomerization. In addition, the ethylene pressure affects the distribution of oligomers significantly. In some cases, the waxes have been obtained and confirmed to be vinyl-terminal long-chain alkenes. Finally, we can conclude that these tridentate iron complexes could be promising catalysts for industrial consideration in ethylene oligomerization for full-range processes.

4. Experimental Section

4.1. General Considerations. All manipulations of air- and moisture-sensitive compounds were performed under a nitrogen atmosphere using standard Schlenk techniques. Toluene was refluxed over sodium−benzophenone and distilled under argon prior to use. Methylaluminoxane (MAO, a 1.46 M solution in toluene) and modified methylaluminoxane (MMAO, 1.93 M in heptane, 3A) were purchased from Akzo Nobel Corp. Diethylaluminum chloride (Et_2AlCl, 1.7 M in toluene) was purchased from Acros Chemicals. Other reagents were purchased from Aldrich or Acros Chemicals; the boiling range of light petroleum is 30−60 °C and the type of silica gel used is 200−300 mesh. ^{1}H and ^{13}C NMR spectra were recorded on a Bruker DMX 300 MHz instrument at ambient temperature using TMS as an internal standard. IR spectra were recorded on a Perkin-Elmer System 2000 FT-IR spectrometer. Elemental analysis was carried out using an HPMOD 1106 microanalyzer. GC analysis was performed with a Carlo Erba Strumentazione gas chromatograph equipped with a flame ionization detector and a 30 m (0.25 mm i.d., 0.25 μm film thickness) DM-1 silica capillary column. The yield of oligomers was calculated by referencing to the mass of the solvent on the basis of the prerequisite that the mass of each fraction was approximately proportional to its integrated area in the GC trace. Selectivity for the linear α-olefin

was defined as (amount of linear α-olefin of all fractions)/(total amount of oligomer products) in percent. ^{1}H and ^{13}C NMR spectra of the PE samples were recorded on a Bruker DMX 300 MHz instrument at 110 °C in 1,2-dichlorobenzene-d_4 using TMS as the internal standard.

4.2. Preparation of the Starting Materials. 4.2.1. Preparation of the Precursor Compounds. 2-(2-Benzimidazolyl)-6-methylpyridine (1). A mixture of equivalent molar amounts of *o*-phenylenediamine (21.6 g, 0.20 mol) and 2,6-lutidine (21.4 g, 0.20 mol) with excess sulfur (22.5 g, 0.70 mol) was heated to 170 °C and stirred for 10 h. After the mixture was cooled to room temperature, 250 mL of methanol was added, and the precipitated solid (including unreacted sulfur) was filtered off. The filtrate was evaporated and recrystallized in benzene to get yellow needlelike crystals as the target compound, yield 26.8 g (**1**) (64%). Mp: 228−230 °C (lit.[26] mp 222.5−223 °C). ^{1}H NMR (300 MHz, $CDCl_3$, TMS): δ 11.2 (s, 1 H, NH), 8.30 (d, 1H, J = 7.9 Hz, Py), 7.70 (m, 2H, Py), 7.20 (m, 4H, Ar), 2.53 (s, 3H, CH_3). IR (KBr; cm^{-1}): 3047, 1598, 1576, 1465, 1416, 1385, 1315, 1279, 1226, 1017, 993, 904, 808, 743, 423.

2-(1-Methyl-2-benzimidazolyl)-6-methylpyridine (2). A solution of **1** (500 mg, 2.39 mmol) in 30 mL of acetonitrile was refluxed with 2 equiv of K_2CO_3 (700 mg, 5.00 mmol) for 0.5 h. Iodomethane (220 μL, 3.35 mmol) was added to this system after the mixture was cooled to room temperature and reacted for 24 h. The mixture was evaporated at reduced pressure, and water (20 mL) was then added, which was extracted with CH_2Cl_2 (4 × 15 mL), and the combined extracts were dried over anhydrous Na_2SO_4 and filtered. The solvent was evaporated at reduced pressure, and the desired compound **2** was obtained as a white solid in 96% yield after purification by column chromatography (silica gel, 3/1 petroleum ether/Et_3N). Mp: 110−111 °C. ^{1}H NMR (300 MHz, $CDCl_3$, TMS): δ 8.17 (d, 1H, J = 7.8 Hz, Py), 7.82 (d, 1H, J = 8.1 Hz, Py), 7.72 (t, 1H, J = 7.8 Hz, Ph), 7.41 (m, 1H, Ph), 7.30 (m, 2H, Ph), 7.19 (d, 1H, J = 7.8 Hz, Py), 4.26 (s, 3H, CH_3), 2.63 (s, 3H, CH_3). ^{13}C NMR (75 MHz, $CDCl_3$, TMS): δ 157.5, 150.7, 150.0, 142.6, 137.4, 137.1, 123.3, 123.2, 122.5, 121.8, 120.0, 109.9, 32.8, 24.6. ESI-MS (*m*/*z*): 224.0 (M + H$^+$). IR (KBr; cm^{-1}): 3058, 2954, 1577, 1472, 1433, 1392, 1372, 1255, 1157, 1077, 1009, 805, 743. Anal. Calcd for $C_{14}H_{13}N_3$ (223.3): C, 75.31; H, 5.87; N, 18.82. Found: C, 74.99; H, 5.79; N, 18.54.

6-(2-Benzimidazolyl)pyridine-2-carboxylic acid (3). 1 (1.50 g, 7.17 mmol) and selenium dioxide (3.60 g, 32.4 mmol) were refluxed in dry pyridine for 36 h. After it was cooled, the mixture was filtered to remove solid Se and the clear solution was evaporated to dryness. The crude residue was suspended in water (50 mL), and the pH was adjusted to 11.0 with NaOH (5 M). The resulting clear yellow solution was extracted with dichloromethane (3 × 25 mL), and the aqueous phase was filtered and neutralized to pH 3.4 with concentrated hydrochloric acid. Thereafter the precipitate was collected by filtration and crystallized from 1/1 dimethyl sulfoxide/water (100 °C) to give 1.12 g (4.68 mmol, yield 66%). Mp: 299−301 °C. ^{1}H NMR (300 MHz, DMSO, TMS): δ 8.55 (d, 1 H, J = 7.6 Hz, Py), 8.20 (m, 2H, Py), 7.71 (m, 2H, Ar), 7.31 (m, 2H, Ar).

2-(Carboethoxy)-6-(2-benzimidazolyl)pyridine (4). 3 (0.50 g, 2.09 mmol) and 1 mL of H_2SO_4 (98%) were refluxed in 40 mL of ethanol for 4 h. After the mixture was cooled to room temperature, it was filtered into 50 mL of water, and then the pH was adjusted to 7.0 with saturated $NaHCO_3$ solution. Then ethanol was evaporated and the aqueous phase was extracted with dichloromethane (3 × 25 mL), the combined organic phases were dried over anhydrous Na_2SO_4 and filtered, and the solvent was evaporated at reduced pressure. The solid was collected and recrystallized from dichloromethane to give 0.44 g (1.63 mmol, yield 78%) of pure compound. Mp: 152−154 °C (lit.[28] mp 148−149 °C). ^{1}H NMR (300 MHz, $CDCl_3$, TMS): δ 12.06 (s, 1 H, NH), 8.60 (d, 1H, J = 7.9 Hz, Py), 8.10 (d, 1H, J = 7.6 Hz, Py), 7.95 (t, 1H, J = 7.7 Hz, Py), 7.82 (s, 1H, Ar), 7.45 (s, 1H, Ar), 7.27 (m, 2H, Ar), 4.45 (q, 2H, CH_2), 1.42 (t, 3H, CH_3). IR (KBr; cm^{-1}): 3068, 1720, 1662, 1594, 1460, 1405, 1367, 1300, 1250, 1228, 1117, 1098, 997, 925, 836, 743, 378.

2-(Carboethoxy)-6-(1-methyl-2-benzimidazolyl)pyridine (5). A solution of **4** (300 mg, 1.12 mmol) in 30 mL of acetonitrile was refluxed with 2 equiv of K_2CO_3 (310 mg, 2.24 mmol) for 0.5 h. After the mixture was cooled to room temperature, iodomethane (100 μL, 1.56 mmol) was added to the reaction mixture and the mixture stirred for 24 h. The solvent was evaporated at reduced pressure before water (20 mL) was added, and the aqueous phase was extracted with CH_2Cl_2 (4 × 15 mL). The combined extracts were dried over anhydrous Na_2SO_4 and filtered, and the solvent was finally evaporated at reduced pressure. The desired compound **5** was obtained as a white solid in 75% yield after purification by column chromatography (silica gel, 3/1 (v/v) petroleum ether/ethyl acetate). Mp: 140−141 °C. ^{1}H NMR (300 MHz, $CDCl_3$, TMS): δ 8.62 (d, 1H, J = 6.6 Hz, Py), 8.14 (d, 1H, J = 6.6 Hz, Py), 8.00 (t, 1H, J = 7.8 Hz, Py);, 7.82 (d, 1H, J = 7.5 Hz, Ar), 7.44 (d, 1H, J = 7.2 Hz, Ar), 7.35 (m, 2H, Ar), 4.48 (q, 2H, J = 7.2 Hz, CH_2), 4.40 (s, 3H, CH_3), 1.47 (t, 3H, J = 7.2 Hz, CH_3). ^{13}C NMR (75 MHz, $CDCl_3$, TMS): δ 165.0, 150.8, 149.2, 147.2, 142.6, 137.9, 137.6, 127.5, 124.8, 123.8, 122.9, 120.3, 110.2, 61.9, 33.0, 14.4. ESI-MS (*m*/*z*): 282.2 (M + H$^+$), 320.1 (M + K$^+$). IR (KBr; cm^{-1}): 3366, 3052, 2978, 2926, 2856, 1730 ($\nu_{C=O}$), 1590, 1473, 1403, 1386, 1300, 1251, 1165, 740. Anal. Calcd for $C_{16}H_{15}N_3O_2$ (281.3): C, 68.31; H, 5.37; N, 14.94. Found: C, 68.42; H, 5.37; N, 14.86.

2-(1-Methyl-2-benzimidazolyl)-6-acetylpyridine (6). A solution of **5** (10.8 g, 43.2 mmol) in 15 mL of freshly distilled ethyl acetate was added dropwise to 5.8 equiv of dried C_2H_5ONa (17.0 g, 250 mmol) with stirring to afford a yellow mixture, which was refluxed for 12 h and allowed to stand overnight. Concentrated HCl (50 mL) was added dropwise with stirring, and the mixture was refluxed for another period of 6 h to complete the reaction. With addition of 200 mL of water, the mixture turned into an orange solution; the aqueous phase was then extracted with CH_2Cl_2 (4 × 50 mL), and the combined extracts were washed with 5% aqueous Na_2CO_3. The organic phase was dried over anhydrous Na_2SO_4 and filtered before the solvent was evaporated at reduced pressure. The desired compound **6** was obtained as a white solid in 59% yield after purification by column chromatography (silica gel, 3/1 (v/v) petroleum ether/ethyl acetate). Mp: 189−190 °C. ^{1}H NMR (300 MHz, $CDCl_3$, TMS): δ 8.62 (d, 1H, J = 7.8 Hz, Py), 8.08 (d, 1H, J = 7.5 Hz, Py), 7.99 (t, 1H, J = 7.5 Hz, Py), 7.83 (d, 1H, J = 7.2 Hz, Ar), 7.45 (d, 1H, J = 7.8 Hz, Ar), 7.35 (m, 2H, Ar), 4.34 (s, 3H, CH_2), 2.78 (s, 3H, CH_3). ^{13}C NMR (75 MHz, $CDCl_3$, TMS): δ 199.4, 152.4, 150.0, 149.3, 142.5, 138.0, 137.4, 128.1, 123.8, 123.0, 121.7, 120.3, 110.0, 33.1, 26.2. ESI-MS (*m*/*z*): 252.3 (M + H$^+$), 274.2 (M + Na$^+$). IR (KBr; cm^{-1}): 3369, 3059, 2960, 1696 ($\nu_{C=O}$), 1583, 1469, 1435, 1387, 1353, 1300, 1261, 1214, 1149, 1106, 1020, 817, 748. Anal. Calcd for $C_{15}H_{13}N_3O$ (251.3): C, 71.70; H, 5.21; N, 16.72. Found: C, 71.98; H, 5.30; N, 16.70.

Synthesis of [2-(2-Benzimidazolyl)-6-methylpyridine]dichloroiron (1a). The ligand **1** (400 mg, 1.91 mmol) and $FeCl_2 \cdot 4H_2O$ (362 mg, 1.82 mmol) were placed in a Schlenk tube, followed by the addition of freshly distilled ethanol (3 mL) with rapid stirring at room temperature. The solution turned yellow immediately, and a yellow powder precipitated after 1 min. The reaction mixture was stirred for 12 h, and after the mixture stood for 30 min, the supernatant was removed. The precipitate was washed with diethyl ether twice and dried under vacuum to give the pure product as a yellow powder in 92% yield. IR (KBr; cm^{-1}): 3229, 1606, 1576, 1492, 1475, 1446, 1401, 1378, 1321, 1247, 1152, 1107, 987, 911, 801, 746, 431. Anal. Calcd for $C_{13}H_{11}Cl_2FeN_3$ (336.0): C, 46.47; H, 3.30; N, 12.51. Found: C, 46.76; H, 3.66; N, 12.26.

Synthesis of [2-(2-Benzimidazolyl)-6-methylpyridine]dichlorocobalt (1b). 1b was synthesized by the same method as for **1a**; the green powder was produced in 79% yield. IR (KBr; cm^{-1}): 3228, 1609, 1575, 1493, 1477, 1440, 1387, 1320, 1297, 1231, 1119, 1102, 985, 934, 800, 761, 744, 429. Anal. Calcd for $C_{13}H_{11}Cl_2CoN_3$ (339.1): C, 46.05; H, 3.27; N, 12.39. Found: C, 46.06; H, 3.36; N, 12.37.

Synthesis of [2-(1-Methyl-2-benzimidazolyl)-6-methylpyridine]dichloroiron (2a). 2a was synthesized by the same method as for **1a**; the yellow powder was produced in 94% yield. IR (KBr; cm^{-1}): 3123, 3064, 1605, 1487, 1443, 1390, 1347, 1249, 1162, 1010, 797, 747. Anal. Calcd for $C_{14}H_{13}Cl_2FeN_3$ (350.0): C, 48.04; H, 3.74; N, 12.00. Found: C, 48.11; H, 3.76; N, 11.80.

Synthesis of [2-(1-Methyl-2-benzimidazolyl)-6-methylpyridine]dichlorocobalt (2b). 2b was synthesized by the same method as for **1a**; the green powder was produced in 77% yield. IR (KBr; cm^{-1}): 3121, 3066, 1606, 1488, 1440, 1392, 1347, 1250, 1163, 1014, 796, 747. Anal. Calcd for $C_{14}H_{13}Cl_2CoN_3$ (353.1): C, 47.62; H, 3.71; N, 11.90. Found: C, 47.42; H, 3.82; N, 11.75.

Synthesis of [2-(Carboethoxy)-6-(2-benzimidazolyl)pyridine]dichloroiron (4a). 4a was synthesized by the same method as for **1a**; the brown powder was produced in 89% yield. IR (KBr; cm^{-1}): 3056, 1668, 1602, 1575, 1476, 1414, 1374, 1334, 1274, 1149, 1077, 993, 815, 762, 374. Anal. Calcd for $C_{15}H_{13}Cl_2FeN_3O_2$ (394.0): C, 45.72; H, 3.33; N, 10.66. Found: C, 45.42; H, 3.13; N, 11.15.

Synthesis of [2-(Carboethoxy)-6-(2-benzimidazolyl)pyridine]dichlorocobalt (4b). 4b was synthesized by the same method as for **1a**; the green powder was produced in 72% yield. IR (KBr; cm^{-1}): 3064, 1743, 1698, 1602, 1471, 1422, 1373, 1326, 1271, 1202, 1153, 1089, 990, 856, 754, 434. Anal. Calcd for $C_{15}H_{13}Cl_2CoN_3O_2$ (397.1): C, 45.37; H, 3.30; N, 10.58. Found: C, 45.00; H, 3.39; N, 10.49.

Synthesis of [2-(Carboethoxy)-6-(1-methyl-2-benzimidazolyl)pyridine]dichloroiron (5a). 5a was synthesized by the same method as for **1a**; the purple powder was produced in 98% yield. IR (KBr; cm^{-1}): 3419, 3063, 1697 ($\nu_{C=O}$), 1597, 1486, 1403, 1376, 1328, 1256, 1013, 862, 754. Anal. Calcd for $C_{16}H_{15}Cl_2FeN_3O_2$ (408.1): C, 47.09; H, 3.71; N, 10.30. Found: C, 46.78; H, 3.66; N, 10.45.

Synthesis of [2-(Carboethoxy)-6-(1-methyl-2-benzimidazolyl)pyridine]dichlorocobalt (5b). 5b was synthesized by the same method as for **1a**; the green powder was produced in 79% yield. IR (KBr; cm^{-1}): 3382, 3063, 1703 ($\nu_{C=O}$), 1598, 1487, 1403, 1376, 1327, 1256, 1201, 1093, 1017, 835, 754. Anal. Calcd for $C_{16}H_{15}Cl_2CoN_3O_2$ (411.1): C, 46.74; H, 3.68; N, 10.22. Found: C, 46.50; H, 3.83; N, 10.24.

Synthesis of [2-Acetyl-6-(1-methyl-2-benzimidazolyl)pyridine]dichloroiron (6a). 6a was synthesized by the same method as for **1a**; the purple powder was produced in 88% yield. IR (KBr; cm^{-1}): 3420, 3035, 1659 ($\nu_{C=O}$), 1593, 1486, 1423, 1347, 1330, 1272, 1249, 1191, 1149, 807, 765, 749. Anal. Calcd for $C_{15}H_{13}Cl_2FeN_3O$ (378.0): C, 47.66; H, 3.47; N, 11.12. Found: C, 47.61; H, 3.72; N, 10.90.

Synthesis of [2-Acetyl-6-(1-methyl-2-benzimidazolyl)pyridine]dichlorocobalt (6b). 6b was synthesized by the same method as for **1a**; the green powder was produced in 85% yield. IR (KBr; cm^{-1}): 3430, 3036, 1673 ($\nu_{C=O}$), 1594, 1487, 1424, 1365, 1330, 1269, 1247, 1191, 1149, 1020, 807, 768. Anal. Calcd for $C_{15}H_{13}Cl_2CoN_3O$ (381.1): C, 47.27; H, 3.44; N, 11.03. Found: C, 47.51; H, 3.76; N, 10.89.

4.3. Synthesis of 2-(1-Methyl-2-benzimidazolyl)-2-(1-(arylimino)ethyl)pyridines (7−11) and Their Iron and Cobalt Complexes. 4.3.1. Synthesis of Tridentate Ligands 7−11. (*E*)-2,6-Dimethyl-*N*-(1-(6-(1-methyl-1*H*-benzo[*d*]imidazol-2-yl)pyridin-2-yl)ethylidene)benzenamine (7). A mixture of 2,6-dimethylaniline (106 mg, 0.88 mmol), **6** (200 mg, 0.80 mmol), and a catalytic amount of *p*-toluenesulfonic acid in toluene (25 mL) was refluxed for 24 h. After solvent evaporation, the crude product was purified by column chromatography on silica gel with petroleum ether/ethyl acetate (3/1 v/v) as eluent to afford the product as a yellow powder in 68% yield. Mp: 170−172 °C. ^{1}H NMR (300 MHz, $CDCl_3$, TMS): δ 8.55 (d, 1H, J = 7.8 Hz, Py), 8.46 (t, 1H, J = 7.5 Hz, Py), 7.96 (t, 1H, J = 7.8 Hz, Py), 7.85 (m, 1H, Ph), 7.44 (d, 1H, Ph), 7.34 (m, 2H, Ph), 7.08 (d, 2H, J = 7.5 Hz, Ph), 6.95 (t, 1H, J = 7.2 Hz, Ph), 4.35 (s, 3H, CH_3), 2.25 (s, 3H, CH_3), 2.06 (s, 6H, CH_3). ^{13}C NMR (75 MHz, CDCl3, TMS): δ 166.7, 155.3, 150.0, 149.6, 148.6, 142.7, 137.6, 137.4, 128.0, 125.9, 125.4, 123.6, 123.3, 122.8, 121.4, 120.2, 110.0, 33.1, 18.1, 16.9. ESI-MS (*m*/*z*): 355.5 (M + H^+), 377.3 (M + Na^+). IR (KBr; cm^{-1}): 3421, 2944, 1645 ($\nu_{C=N}$), 1592, 1571, 1541, 1468, 1384, 1361, 1328, 1205, 1149, 1115, 770, 747. Anal. Calcd for $C_{23}H_{22}N_4$ (354.5): C, 77.94; H, 6.26; N, 15.81. Found: C, 77.71; H, 6.37; N, 15.52.

(*E*)-2,6-Diethyl-*N*-(1-(6-(1-methyl-1*H*-benzo[*d*]imidazol-2-yl)-pyridin-2-yl)ethylidene)benzenamine (8). Using the same procedure as for the synthesis of **7**, **8** was obtained as a yellow powder in 89% yield. Mp: 181−182 °C. ^{1}H NMR (300 MHz, $CDCl_3$, TMS): δ 8.56 (d, 1H, J = 7.8 Hz, Py), 8.45 (d, 1H, J = 8.1 Hz, Py), 7.98 (t, 1H, J = 7.8 Hz, Ph), 7.86 (m, 1H, Ph), 7.45 (d, 1H, J = 6.0 Hz, Ph), 7.35 (m, 2H, Ph), 7.14 (d, 2H, J = 8.1 Hz, Ph), 7.05 (m, 1H, Ph), 4.36 (s, 3H, CH_3), 2.40 (q, 4H, J = 7.5 Hz, CH_2), 2.27 (s, 3H, CH_3), 1.15 (t, 6H, J = 7.5 Hz, CH_3). ^{13}C NMR (75 MHz, $CDCl_3$, TMS): δ 166.4, 155.4, 150.0, 149.5, 147.7, 142.5, 137.6, 137.3, 131.2, 126.1, 125.9, 123.6, 123.5, 122.9, 121.4, 120.2, 110.0, 33.1, 24.7, 17.3, 13.9. ESI-MS (*m*/*z*): 383.5 (M + H^+). IR (KBr; cm^{-1}): 3060, 2965, 2931, 2872, 1917, 1639 ($\nu_{C=N}$), 1588, 1570, 1469, 1453, 1432, 1396, 1358, 1329, 1252, 1198, 1153, 1113, 1072, 758, 741. Anal. Calcd for $C_{25}H_{26}N_4$ (382.5): C, 78.50; H, 6.85; N, 14.65. Found: C, 78.20; H, 6.84; N, 14.55.

(*E*)-2,6-Diisopropyl-N-(1-(6-(1-methyl-1*H*-benzo[*d*]imidazol-2-yl)pyridin-2-yl)ethylidene)benzenamine (9). Using the same procedure as for the synthesis of **7**, **9** was obtained as a yellow powder in 86% yield. Mp: 222 −223 °C. ^{1}H NMR (300 MHz, $CDCl_3$, TMS): δ 8.44 (d, 1H, J = 7.8 Hz, Py), 8.35 (t, 1H, J = 7.5 Hz, Py), 7.85 (t, 1H, J = 7.8 Hz, Ph), 7.76 (d, 1H, J = 6.1 Hz, Ph), 7.33 (d, 1H, J = 6.1 Hz, Ph), 7.22 (m, 2H, Ph), 7.09 (m, 2H, Ph), 7.00 (m, 1H, Ph), 4.24 (s, 3H, CH_3), 2.68 (m, 2H, CH), 2.19 (s, 3H, CH_3), 1.09 (d, 12H, J = 6.6 Hz, CH_3). ^{13}C NMR (75 MHz, $CDCl_3$, TMS): δ 166.5, 155.4, 150.0, 149.6, 146.4, 142.7, 137.6, 137.4, 135.8, 125.9, 123.9, 123.5, 123.2, 122.8, 121.4, 120.2, 110.0, 33.2, 28.5, 23.3, 23.0, 17.7. ESI-MS (*m*/*z*): 411.5 (M + H^+), 433.5 (M + Na^+). IR (KBr; cm^{-1}): 2961, 1643 ($\nu_{C=N}$), 1570, 1467, 1432, 1393, 1359, 1330, 1262, 1193, 1153, 1110, 1069, 784, 758, 732. Anal. Calcd for $C_{27}H_{30}N_4$ (410.6): C, 78.99; H, 7.37; N, 13.65. Found: C, 79.24; H, 7.11; N, 13.31.

(*E*)-2,6-Dichloro-*N*-(1-(6-(1-methyl-1*H*-benzo[*d*]imidazol-2-yl)pyridin-2-yl)ethylidene)benzenamine (10). Using the same procedure as for the synthesis of **7**, **10** was obtained as a yellow powder in 22% yield. Mp: 178−179 °C. ^{1}H NMR (300 MHz, $CDCl_3$, TMS): δ 8.59 (d, 1H, J = 7.2 Hz, Py), 8.47 (d, 1H, J = 7.2 Hz, Py), 8.00 (t, 1H, J = 7.5 Hz, Py), 7.87 (m, 1H, Ph), 7.45 (m, 1H, Ph), 7.36 (m, 4H, Ph), 7.03 (m, 1H, Ph), 4.36 (s, 3H, CH_3), 2.38 (s, 3H, CH_3).^{13}C NMR (75 MHz, $CDCl_3$, TMS): δ 170.77, 154.5, 149.8, 149.7, 145.6, 142.6, 137.7, 137.4, 128.3, 126.5, 124.6, 124.5, 123.6, 122.8, 122.1, 120.3, 109.9, 33.1, 18.01. ESI-MS (*m*/*z*): 396.2 (M + H^+), 418.0 (M + Na^+). IR (KBr; cm^{-1}): 2924, 1650 ($\nu_{C=N}$), 1587, 1470, 1433, 1393, 1361, 1311, 1265, 1223, 1150, 1112, 1073, 771, 742. Anal. Calcd for $C_{21}H_{16}Cl_2N_4$ (395.3): C, 63.81; H, 4.08; N, 14.17. Found: C, 63.61; H, 4.14; N, 13.94.

(*E*)-2,6-Dibromo-*N*-(1-(6-(1-methyl-1*H*-benzo[*d*]imidazol-2-yl)pyridin-2-yl)ethylidene)benzenamine (11). Using the same procedure as for the synthesis of **7**, **11** was obtained as a yellow powder in 25% yield. Mp: 157−158 °C. ^{1}H NMR (300 MHz, $CDCl_3$, TMS): δ 8.50 (d, 1H, J = 7.2 Hz, Py), 8.39 (d, 1H, J =

Table 9. Crystal Data and Structure Refinement Details

	1b	2a	2b	5b	7
empirical formula	$C_{13}H_{11}Cl_2CoN_3$	$C_{17}H_{20}Cl_2FeN_4O$	$C_{14}H_{13}Cl_2CoN_3$	$C_{16}H_{15}Cl_2CoN_3O_2$	$C_{23}H_{22}N_4$
formula wt	339.08	423.12	353.10	411.14	354.45
cryst color	blue	brown	blue	green	yellow
temp (K)	293(2)	293(2)	293(2)	293(2)	293(2)
wavelength (Å)	0.710 73	0.710 73	0.710 73	0.710 73	0.710 73
cryst syst	monoclinic	monoclinic	monoclinic	triclinic	monoclinic
space group	$P2_1/n$	$P2_1/c$	$P2_1/m$	$P\bar{1}$	$P2_1/c$
a (Å)	7.25050(1)	7.8858(2)	8.6204(2)	7.7749(3)	17.8207(3)
b (Å)	15.3040(3)	16.8075(4)	7.4012(2)	8.3615(2)	8.34060(1)
c (Å)	12.4512(2)	14.1633(4)	12.1953(3)	13.3453(4)	13.2319(2)
α (deg)	90.0	90.0	90.0	92.052(2)	90
β (deg)	91.2860(1)	94.2910(1)	107.8400(1)	93.674(2)	100.7490(1)
γ (deg)	90.0	90.0	90.0	99.584(2)	90
V (Å^3)	1381.26(4)	1871.95(8)	740.66(3)	852.76(5)	1932.22(5)
Z	4	4	2	2	4
D_{calcd} (g cm^{-3})	1.631	1.501	1.583	1.601	1.218
μ (mm^{-1})	1.616	1.104	1.511	1.333	0.074
F(000)	684	872	358	418	752
cryst size (mm)	0.32 × 0.23 × 0.15	0.45 × 0.40 × 0.40	0.45 × 0.32 × 0.10	0.35 × 0.25 × 0.14	0.40 × 0.30 × 0.30
θ range (deg)	2.11−28.30	1.88−28.29	2.56−28.28	2.47−28.32	1.16−28.29
limiting indices	$-9 \le h \le 8$ $-20 \le k \le 20$ $-16 \le l \le 16$	$-10 \le h \le 9$ $-21 \le k \le 22$ $-18 \le l \le 18$	$-11 \le h \le 11$ $-9 \le k \le 9$ $-16 \le l \le 15$	$-10 \le h \le 10$ $-11 \le k \le 11$ $-17 \le l \le 17$	$-23 \le h \le 23$ $-10 \le k \le 10$ $-15 \le l \le 17$
no. of rflns collected	13 866	18 954	6510	11 290	18 748
no. of unique rflns	3286	4650	1963	4193	4745
completeness to θ (%)	95.6 (θ = 28.30°)	99.9 (θ = 28.29°)	99.4 (θ = 28.28°)	98.7 (θ = 28.32°)	99.2 (θ = 28.29°)
abs cor	empirical	empirical	empirical	empirical	empirical
no. of params	176	226	119	217	244
goodness of fit on F^2	1.056	1.063	0.982	1.029	1.042
final R indices ($I > 2\sigma(I)$)	R1 = 0.0278 wR2 = 0.0766	R1 = 0.0391 wR2 = 0.1040	R1 = 0.0269 wR2 = 0.0791	R1 = 0.0367 wR2 = 0.0927	R1 = 0.0468 wR2 = 0.1499
R indices (all data)	R1 = 0.0388 wR2 = 0.0813	R1 = 0.0631 wR2 = 0.1124	R1 = 0.0327 wR2 = 0.0825	R1 = 0.0675 wR2 = 0.1008	R1 = 0.0606 wR2 = 0.1705
largest diff peak, hole (e Å^{-3})	0.381, −0.269	0.441, −0.363	0.357, −0.282	0.442, −0.281	0.254, −0.345

	10	7a	10a	7b	8b	10b
empirical formula	$C_{21}H_{16}Cl_2N_4$	$C_{23}H_{22}Cl_2FeN_4O$	$C_{21}H_{16}Cl_4FeN_4$	$C_{23}H_{22}Cl_2CoN_4$	$C_{25}H_{26}Cl_2CoN_4$	$C_{21}H_{16}Cl_4CoN_4$
formula wt	395.28	497.20	522.03	484.28	512.33	525.11
cryst color	yellow	blue	blue	dark	green	green
temp (K)	293(2)	293(2)	293(2)	293(2)	293(2)	293(2)
wavelength (Å)	0.710 73	0.710 73	0.710 73	0.710 73	0.710 73	0.710 73
cryst syst	orthorhombic	monoclinic	monoclinic	monoclinic	monoclinic	monoclinic
space group	$Pbcn$	$P2_1/n$	$P2_1/c$	$P2_1/c$	$P2_1/c$	$P2_1/c$
a (Å)	17.9085(5)	12.8592(9)	10.2210(3)	8.14280(1)	9.57290(1)	10.1894(3)
b (Å)	8.3223(2)	8.8271(6)	15.1437(4)	15.0548(2)	14.1768(2)	15.1037(5)
c (Å)	25.3872(7)	23.0969(2)	14.1708(4)	18.0755(3)	18.5031(3)	14.1505(4)
β (deg)	90	101.934(4)	97.857(2)	96.1460(1)	95.5010(1)	98.085(2)
V (Å^3)	3783.71(2)	2565.1(3)	2172.82(1)	2203.11(5)	2499.55(6)	2156.08(1)
Z	8	4	4	4	4	4
D_{calcd} (g cm^{-3})	1.388	1.287	1.596	1.460	1.361	1.618
μ (mm^{-1})	0.356	0.816	1.202	1.039	0.920	1.308
F(000)	1632	1024	1056	996	1060	1060
cryst size (mm)	0.95 × 0.85 × 0.80	0.32 × 0.21 × 0.15	0.30 × 0.20 × 0.10	0.40 × 0.30 × 0.30	0.30 × 0.20 × 0.10	0.40 × 0.30 × 0.20
θ range (deg)	1.97−28.32	1.80−28.40	1.98−28.34	2.27−28.28	1.81−28.30	1.98−28.29
limiting indices	$-20 \le h \le 23$ $-10 \le k \le 11$ $-30 \le l \le 33$	$-17 \le h \le 17$ $-11 \le k \le 11$ $-30 \le l \le 30$	$-13 \le h \le 13$ $-20 \le k \le 20$ $-18 \le l \le 18$	$-10 \le h \le 9$ $-20 \le k \le 18$ $-24 \le l \le 23$	$-12 \le h \le 12$ $-18 \le k \le 18$ $-20 \le l \le 24$	$-13 \le h \le 13$ $-20 \le k \le 19$ $-16 \le l \le 18$
no. of rflns collected	20 694	25 506	21 486	22 817	36 642	21 694
no. of unique rflns	4702	6347	5404	5419	6200	5338
completeness to θ (%)	99.7 (θ = 28.32°)	98.6 (θ = 28.40°)	99.7 (θ = 28.34°)	99.1 (θ = 28.28°)	99.8 (θ = 28.30°)	99.4 (θ = 28.29°)
abs cor	empirical	empirical	empirical	empirical	empirical	empirical
no. of params	244	289	271	271	271	271
goodness of fit on F^2	0.944	0.822	1.058	1.048	1.087	1.084
final R indices ($I > 2\sigma(I)$)	R1 = 0.0447 wR2 = 0.1215	R1 = 0.0592 wR2 = 0.1823	R1 = 0.0434 wR2 = 0.1094	R1 = 0.0317 wR2 = 0.0897	R1 = 0.0577 wR2 = 0.1801	R1 = 0.0309 wR2 = 0.0860
R indices (all data)	R1 = 0.0961 wR2 = 0.1370	R1 = 0.1821 wR2 = 0.2183	R1 = 0.0803 wR2 = 0.1234	R1 = 0.0374 wR2 = 0.0934	R1 = 0.0789 wR2 = 0.1963	R1 = 0.0415 wR2 = 0.0910
largest diff peak, hole (e Å^{-3})	0.301, −0.342	0.558, −0.386	0.374, −0.432	0.565, −0.568	1.050, −1.488	0.477, −0.503

7.2 Hz, Py), 7.93 (t, 1H, $J = 7.2$ Hz, Py), 7.79 (d, 1H, $J = 6.3$ Hz, Ph), 7.51 (d, 2H, $J = 7.5$ Hz, Ph), 7.25 (m, 3H, Ph), 6.78 (m, 1H, Ph), 4.28 (s, 3H, CH_3), 2.28 (s, 3H, CH_3).^{13}C NMR (75 MHz, $CDCl_3$, TMS): δ 170.6, 154.5, 149.9, 149.8, 148.0, 142.6, 137.8, 137.4, 132.1, 126.5, 125.5, 123.6, 122.9, 122.1, 120.3, 113.7, 101.0, 33.1, 18.1. ESI-MS (*m*/*z*): 485.0 ($M + H^+$). IR (KBr; cm^{-1}): 2953, 1647 ($\nu_{C=N}$), 1587, 1468, 1428, 1362, 1313, 1265, 1222, 1150, 1114, 1073, 825, 747. Anal. Calcd for $C_{21}H_{16}Br_2N_4$ (484.2): C, 52.09; H, 3.33; N, 11.57. Found: C, 52.38; H, 3.53; N, 11.27.

4.3.2. Synthesis of Tridentate Iron Complexes 7a−11a. The complexes **7a**−**11a** were synthesized by the reaction of $FeCl_2{\cdot}4H_2O$ with the corresponding ligands in ethanol. A typical synthetic procedure for **7a** can be described as follows. The ligand **7** (150 mg, 0.42 mmol) and $FeCl_2{\cdot}4H_2O$ (79.5 mg, 0.40 mmol) were added to a Schlenk tube, followed by the addition of freshly distilled ethanol (2 mL) with rapid stirring at room temperature. The solution turned deep blue immediately, and a blue powder was formed after 1 min. The reaction mixture was stirred for 10 h and allowed to stand for 30 min before the supernatant was removed. The precipitate was washed with diethyl ether twice and dried under vacuum to give the pure product as a blue powder in 96% yield. IR (KBr; cm^{-1}): 3449, 2951, 2915, 1594 ($\nu_{C=N}$), 1487, 1470, 1399, 1372, 1284, 1348, 1331, 1259, 1209, 1098, 794, 748. Anal. Calcd for $C_{23}H_{22}Cl_2FeN_4$ (481.2): C, 57.41; H, 4.61; N, 11.64. Found: C, 57.09; H, 4.30; N, 11.41. Data for **8a** are as follows. Yield: 89%. IR (KBr; cm^{-1}): 3398, 2962, 2932, 2875, 1595 ($\nu_{C=N}$), 1486, 1445, 1422, 1398, 1371, 1349, 1304, 1284, 1256, 1162, 1126, 792, 754. Anal. Calcd for $C_{25}H_{26}Cl_2FeN_4$ (509.3): C, 58.96; H, 5.15; N, 11.00. Found: C, 59.06; H, 5.08; N, 10.75. Data for **9a** are as follows. Yield: 95%. IR (KBr; cm^{-1}): 3423, 2963, 2929, 2869, 1595 ($\nu_{C=N}$), 1487, 1464, 1444, 1399, 1369, 1351, 1283, 1255, 1199, 1106, 792, 757. Anal. Calcd for $C_{27}H_{30}Cl_2FeN_4$ (537.3): C, 60.35; H, 5.63; N, 10.43. Found: C, 60.50; H, 5.80; N, 10.16. Data for **10a** are as follows. Yield: 70%. IR (KBr; cm^{-1}): 3423, 3057, 1595 ($\nu_{C=N}$), 1562, 1485, 1438, 1396, 1367, 1307, 1282, 1228, 1188, 1159, 1091, 789, 746. Anal. Calcd for $C_{21}H_{16}Cl_4FeN_4$ (522.0): C, 48.32; H, 3.09; N, 10.73. Found: C, 48.40; H, 3.02; N, 10.51. Data for **11a** are as follows. Yield: 72%. IR (KBr; cm^{-1}): 3422, 3063, 1595 ($\nu_{C=N}$), 1552, 1485, 1432, 1395, 1368, 1307, 1259, 1225, 1159, 815, 786, 749, 729. Anal. Calcd for $C_{21}H_{16}Cl_2Br_2FeN_4$ (610.9): C, 41.28; H, 2.64; N, 9.17. Found: C, 41.26; H, 2.24; N, 9.15.

4.3.3. Synthesis of Tridentate Cobalt Complexes 7b−11b. 7b−**11b** were prepared by the same synthetic procedures as for **7a**−**11a** and were obtained as green powders. The synthetic procedure of **7b** can be described as follows: to a mixture of ligand **7** (150 mg, 0.42 mmol) and $CoCl_2$ (52 mg, 0.40 mmol) was added freshly distilled ethanol (2 mL) at room temperature. The solution turned green immediately. The reaction mixture was stirred for 10 h, and the precipitate was collected by filtration and washed with diethyl ether, followed by drying under vacuum. The desired complex was obtained as a green powder in 60% yield. IR (KBr; cm^{-1}): 3440, 2916, 1662, 1594 ($\nu_{C=N}$), 1566, 1488, 1399, 1363, 1329, 1257, 1211, 1156, 1097, 1020, 794, 751. Anal. Calcd for $C_{23}H_{22}Cl_2N_4Co$ (484.3): C, 57.04; H, 4.58; N, 11.57. Found: C, 56.83; H, 4.75; N, 11.46. Data for **8b** are as follows. Yield: 72%. IR (KBr; cm^{-1}): 3446, 3060, 2961, 2874, 1594 ($\nu_{C=N}$), 1487, 1445, 1401, 1369, 1306, 1282, 1256, 1163, 1090, 1024, 793, 757. Anal. Calcd for $C_{25}H_{26}Cl_2N_4Co$ (512.3): C, 58.61; H, 5.12; N, 10.94. Found: C, 58.52; H, 5.21; N, 10.73. Data for **9b** are as follows. Yield: 48%. IR (KBr; cm^{-1}): 3449, 3113, 2963, 2869, 1595 ($\nu_{C=N}$), 1572, 1488, 1461, 1402, 1384, 1329, 1283, 1256, 1201, 1104, 793, 758. Anal. Calcd for $C_{27}H_{30}Cl_2CoN_4$ (540.4): C, 60.01; H, 5.60; N, 10.37. Found: C, 60.11; H, 5.75; N, 10.16. Data for **10b** are as follows. Yield: 57%. IR (KBr; cm^{-1}): 3445, 3053, 2362, 1596 ($\nu_{C=N}$), 1573, 1488, 1434, 1401, 1365, 1307, 1283, 1258, 1231, 1191, 1160, 1090, 1021, 789, 763. Anal. Calcd for $C_{21}H_{16}Cl_4N_4Co$ (525.1): C, 48.03; H, 3.07; N, 10.67. Found: C, 47.78; H, 3.20; N, 10.61. Data for **11b** are as follows. Yield: 46%. IR (KBr; cm^{-1}): 3422, 3061, 1595 ($\nu_{C=N}$), 1486, 1432, 1370, 1333, 1281, 1259, 1227, 1187, 1160, 1094, 815, 789, 748, 730. Anal. Calcd for $C_{21}H_{16}Cl_2Br_2CoN_4$ (614.0): C, 41.08; H, 2.63; N, 9.12. Found: C, 41.27; H, 2.27; N, 9.00.

4.6. Procedure for Ethylene Oligomerization and Polymerization. Ethylene oligomerization and polymerization were performed in a stainless steel autoclave (0.5 L capacity) equipped with a gas ballast through a solenoid clave for continuous feeding of ethylene at constant pressure. A 100 mL amount of toluene containing the catalyst precursor was transferred to the fully dried reactor under a nitrogen atmosphere. The required amount of cocatalyst (MAO, MMAO, or Et_2AlCl) was then injected into the reactor via a syringe. At the reaction temperature, the reactor was sealed and pressurized to high ethylene pressure, and the ethylene pressure was maintained with feeding of ethylene. After the reaction mixture was stirred for the desired period, the pressure was released and a small amount of the reaction solution was collected, which was then analyzed by gas chromatography (GC) for determining the composition and mass distribution of oligomers obtained. Then the residual reaction solution was quenched with 5% hydrochloric acid in ethanol. The precipitated low-molecular-weight waxes were collected by filtration, washed with ethanol and water, and dried under vacuum to constant weight.

4.7. X-ray Crystallographic Studies. Single-crystal X-ray diffraction studies for **1b**, **2a**, **2b**, **5b**, **7**, **10**, **7a**, **10a**, **7b**, **8b**, and **10b** were carried out on a Bruker SMART 1000 CCD diffractometer with graphite-monochromated Mo Kα radiation ($\lambda = 0.710\ 73$ Å). Cell parameters were obtained by global refinement of the positions of all collected reflections. Intensities were corrected for Lorentz and polarization effects and empirical absorption. The structures were solved by direct methods and refined by full-matrix least squares on F^2. All non-hydrogen atoms were refined anisotropically. All hydrogen atoms were placed in calculated positions. Structure solution and refinement were performed by using the SHELXL-97 package.[41] Crystal data and processing parameters for **1b**, **2a**, **2b**, **5b**, **7**, **10**, **7a**, **10a**, **7b**, **8b**, and **10b** are summarized in Table 9.

Acknowledgment. This work was supported by NSFC No. 20674089 and MOST No. 2006AA03Z553. We thank Mr. Sherrif Adewuyi for the English corrections.

Supporting Information Available: CIF files giving X-ray crystallographic data for **1b**, **2a**, **2b**, **5b**, **7**, **10**, **7a**, **10a**, **7b**, **8b**, and **10b**, along with text and figures giving representative examples of $\pi-\pi$ stacking and hydrogen bonding between two adjacent molecules. This material is available free of charge via the Internet at http://pubs.acs.org.

OM0700819

(41) Sheldrick, G. M. SHELXTL-97, Program for the Refinement of Crystal Structures; University of Göttingen, Göttingen, Germany, 1997.